ACCSCIENCE PUBLISHING

International Journal of Bioprinting

REVIEW ARTICLE

Acoustic-assisted hydrogel fabrication, 3D printing, and 3D bioprinting

Zichuan Ding†, Yiyuan Wang†, Jiaxuan Fan, Ying Hong, Xiao Rong*, and Li Qiu*

Department of Ultrasound, West China Hospital, Sichuan University, Chengdu, Sichuan, China

Abstract

Hydrogels, three-dimensional (3D) printing, and 3D bioprinting hold considerable promise for biomedical applications. Compared to conventional hydrogel fabrication strategies triggered by light, heat, or crosslinking agents, acoustic-assisted hydrogel fabrication, 3D printing, and 3D bioprinting offer unique advantages, including superior tissue penetration, high spatiotemporal controllability, and enhanced biosafety. This review systematically elucidates the significant potential and innovative mechanisms of ultrasound as a unique physical stimulus in these fields. This review highlights the fundamental principles of acoustic effects—cavitation, mechanical effects, and thermal effects—and their roles in hydrogel preparation. We then comprehensively discuss the multiple pathways for acoustic-assisted hydrogel fabrication, including cavitation-triggered free-radical polymerization, mechanically/thermally induced polymerization, liposome-mediated and enzyme-catalyzed polymerization, self-assembly systems for polymerization, and homogenization effects in polymerization, highlighting their respective applications in biomedicine and other related fields. Subsequently, advances in the emerging field of acoustic-assisted 3D printing and 3D bioprinting are reviewed in detail, ranging from the acoustic triggering of 3D printing with thermally curable/free-radical polymerization inks to micrometer-scale 3D bioprinting using cell-laden bioinks. Finally, this review highlights current bottlenecks and future research directions in acoustic-assisted hydrogel fabrication, 3D printing, and 3D bioprinting.

Keywords: Ultrasound; Acoustic effects; Hydrogel; Three-dimensional printing; Three-dimensional bioprinting

†*These authors contributed equally to this work.*

***Corresponding authors:**
Xiao Rong (rongxiao@scu.edu.cn)
Li Qiu (qiulihx@scu.edu.cn)

Citation: Ding Z, Wang Y, Fan J, Hong Y, Rong X, Qiu L. Acoustic-assisted hydrogel fabrication and 3D (bio)printing. *Int J Bioprint*. 2026;12(3):026070058. doi: 10.36922/IJB026070058

Received: February 10, 2026

Revised: March 6, 2026

Accepted: March 11, 2026

Published Online: April 22, 2026

1. Introduction

Hydrogels are three-dimensional (3D) polymeric networks capable of absorbing and retaining substantial amounts of water without dissolution.[1] A pivotal step in their preparation involves the transition from a liquid precursor solution to a solid gel, a process termed crosslinking, which fundamentally dictates hydrogel formation and final properties.[2] The crosslinked network provides structural integrity, while the water molecules confined within it create an environment akin to the extracellular matrix. Crosslinking essentially connects linear or branched polymer chains via chemical bonds (chemical crosslinking) or physical interactions (physical crosslinking), forming the crucial 3D network, which is essentially a process of macromolecular polymerization.[3]

Chemical crosslinking, typically involving covalent or dynamic covalent bonds, results in permanent networks known for their stability and superior mechanical strength.[4,5] In contrast, physical crosslinking relies on reversible non-covalent interactions such as hydrogen bonding, ionic interactions, and hydrophobic associations, yielding networks with relatively weaker stability.[6] Consequently, a pivotal aspect of hydrogel fabrication is the method used to trigger crosslinking—that is, the external or internal stimulus that initiates or drives the gelation process through polymerization among polymer molecules in the precursor solution. Common triggers include light, heat, crosslinking agents, and free radicals.[7] The selected fabrication method determines the gelation kinetics, spatial resolution, biocompatibility, and ultimate application. For instance, while photocrosslinking offers exceptional precision, concerns regarding limited tissue penetration depth and potential cytotoxicity persist.

Furthermore, the optimal trigger varies depending on whether the hydrogel is derived from natural polymers (e.g., collagen, polysaccharides) or synthetic polymers (e.g., polyethylene glycol, polyacrylamide, polyvinyl alcohol). Owing to their excellent biocompatibility and tunable physicochemical properties, hydrogels hold an indispensable position in biomedical engineering, serving as 3D scaffolds for tissue regeneration,[8] carriers for organoid culture in drug screening,[9] and components in flexible electronics for conduction and sensing.[10] Equally noteworthy are advanced fabrication strategies such as 3D bioprinting, in situ crosslinking, microfluidics, and electrospinning, which enable the production of hydrogels with diverse architectures, properties, and functions.[11]

Three-dimensional printing, an advanced additive manufacturing technology, has revolutionized manufacturing by enabling the precise fabrication of complex, customized structures.[12] In biomanufacturing and biomedicine, 3D bioprinting has attracted significant interest.[13] Its core principle involves using additive manufacturing techniques to fabricate predefined 3D models into tissue- or organ-like scaffolds with complex architectures and functions, utilizing hydrogels (bioinks) laden with living cells and bioactive molecules.[14] Although 3D bioprinting integrates computer science, materials science, and cell biology, its foremost tenet is maintaining the viability and function of cells within the bioink, which is critical for successful biomedical applications.[15,16]

Modulating the properties of hydrogel matrices, whether natural or synthetic, is thus a decisive factor in preserving overall bioactivity and ensuring successful bioprinting. Predominant bioprinting technologies include extrusion-based, vat photopolymerization (e.g., stereolithography), and inkjet-based printing. Extrusion-based printing deposits bioinks through a nozzle via layer-by-layer stacking, offering a simple principle, a controllable process, and suitability for viscous inks.[17,18] However, its resolution is limited, and the shear forces generated during extrusion can damage cells. Photopolymerization employs a nozzle-free approach, using light projection to pattern and cure photosensitive materials layer by layer. It boasts high resolution, fast printing speed, and minimal cell damage, but is restricted to photoresponsive materials.[19,20] A key limitation common to these prevalent techniques is the restricted tissue penetration depth of their triggering stimuli (e.g., light). Even near-infrared light, which offers the deepest penetration among optical methods, falls short of enabling true in situ manufacturing within the body for tissue engineering.[21] In situ fabrication allows for the minimally invasive delivery of bioinks directly to a defect site, potentially reducing complications associated with surgical implantation, such as infection, hematoma, poor healing, or damage to surrounding tissues.[22]

Ultrasound, a longitudinal wave capable of interacting with various materials through diverse physical and chemical effects, has long been used in imaging and therapy.[23-25] Recently, significant progress has been made in acoustic-assisted fabrication technologies, particularly in hydrogel polymerization and corresponding 3D bioprinting.[26,27] Acoustic-assisted hydrogel fabrication leverages ultrasound-induced physicochemical effects—such as acoustic cavitation, acoustic radiation force, acoustic streaming, and thermal effects—to trigger, modulate, or enhance the polymerization process of precursor solutions.[28] Acoustic-assisted 3D printing and 3D bioprinting of hydrogels constitute an advanced subset of the field. While both rely on ultrasound's physicochemical effects to trigger polymerization, the 3D printing modality places greater emphasis on the spatial structuring process, aiming to achieve "gelation with a predefined, complex 3D architecture." For bioinks used in acoustic-assisted 3D printing and 3D bioprinting, demands for crosslinking precision and speed are higher, heavily reliant on the ink's ultrasound responsiveness to achieve high spatial resolution and rapid fabrication. Compared to traditional crosslinking stimuli such as light or heat, ultrasound offers distinct advantages of non-invasiveness, deep-tissue penetration, excellent spatiotemporal controllability, and biocompatibility, presenting a broader prospect for biomedical applications.[29,30]

However, a systematic review that comprehensively addresses ultrasound-mediated hydrogel polymerization, 3D printing, and 3D bioprinting is currently lacking. Prior literature includes only a few reviews on hydrogel

fabrication strategies that mention ultrasound-triggered hydrogel formation in a sporadic manner.[31,32] To the best of our knowledge, there is still no review that provides a systematic and in-depth discussion of studies on ultrasound-assisted hydrogel fabrication. In this review, starting from the underlying acoustic mechanisms, we comprehensively summarize and classify ultrasound-triggered gelation/polymerization pathways, and further link these pathways to acoustic-assisted 3D printing and 3D bioprinting technologies for in situ fabrication. Garciamendez-Mijares *et al.*[33] have reviewed acoustic-assisted techniques in droplet-based, light-polymerization–based, and extrusion-based bioprinting, and summarized deep-penetration ultrasound polymerization methods as emerging examples. Our review fills the gap in ultrasound-assisted hydrogel fabrication, and these insights may, in turn, inform and potentially reshape the development of ultrasound-based 3D printing approaches (Figure 1).

2. Basic mechanisms

2.1. Acoustic cavitation

Acoustic cavitation is a unique physical phenomenon triggered by oscillating sound pressure in liquid media, centered on the dynamic formation, oscillation, and collapse of cavitation bubbles.[34] It originates when intense, alternating acoustic pressure (particularly during the rarefaction/negative pressure phase) locally reduces the pressure below the liquid's saturated vapor pressure or gas solubility limit, effectively "tearing" the liquid apart to form microscopic cavities (cavitation bubbles) filled with vapor or dissolved gas.[35] These bubbles typically nucleate preferentially at heterogeneous sites within the medium, such as solid particle surfaces, suspended impurities, pre-existing microbubbles, or hydrophobic interfaces. The onset of cavitation has a minimum pressure threshold dependent on ultrasound frequency, liquid properties (e.g., viscosity, surface tension, gas content), ambient pressure, and temperature.[36] Generally, lower frequencies facilitate cavitation. The mechanical index (MI), a key dimensionless parameter in clinical and research settings, is used to assess the potential risk of bioeffects associated with cavitation.[37,38] The MI is calculated as the derated in situ peak negative pressure (PnP) divided by the square root of the center frequency (F_c) as **Equation 1**:

$$MI = \frac{PnP}{\sqrt{F_c}} \quad (1)$$

where the units of PnP and F_c are MPa and MHz, respectively.

Based on the value of MI, cavitation is categorized into stable and inertial types. At lower acoustic pressures (typically MI < 0.4–0.5), bubbles undergo periodic, nonlinear stable oscillations about an equilibrium radius over hundreds to thousands of acoustic cycles without violent collapse, termed stable cavitation.[39] At higher acoustic pressures (typically MI > 0.7), bubbles are violently compressed during the compression/positive

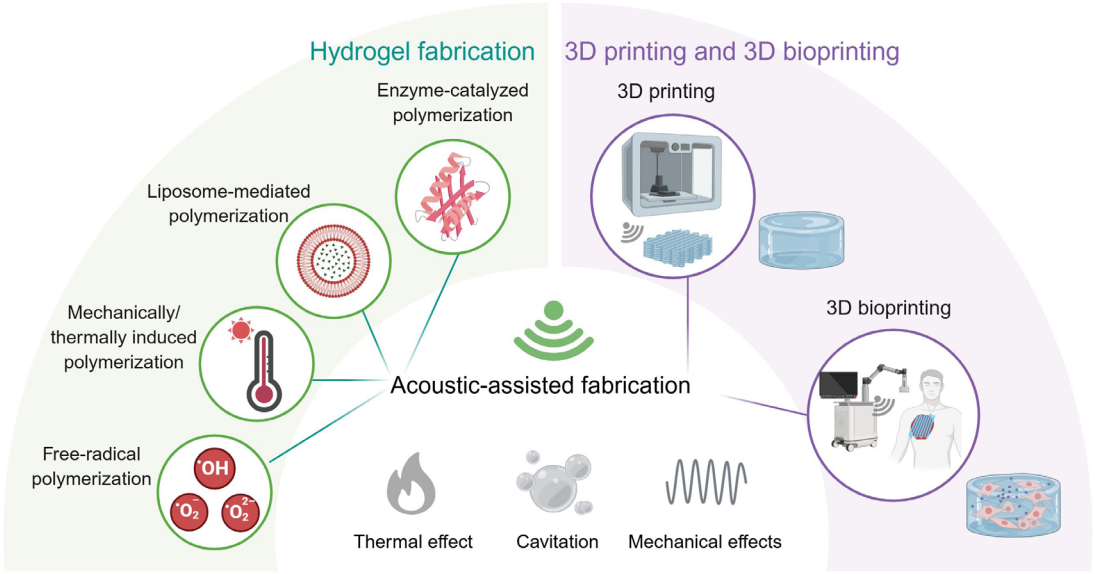

Figure 1. Acoustic-assisted hydrogel fabrication and 3D printing/bioprinting and their underlying basic mechanisms
Abbreviation: 3D: Three-dimensional. Created in BioRender. Rong, X. (2026) https://BioRender.com/ivtfhvn.

pressure phase, failing to sustain stable oscillations and collapsing intensely within one or a few cycles; this is known as inertial cavitation.[40,41]

At the final stage of inertial collapse, transient extremes are generated within the bubble: ultra-high temperatures (>5,000 K), pressures (>1,000 atm), and high-speed microjets (reaching hundreds of meters per second). The intense mechanical effects can cause physical disruption to nearby cells, tissues, or drug carriers, while the high temperature and pressure can induce pyrolysis of water vapor inside the bubble, generating highly reactive free radicals (e.g., hydroxyl radical [•OH], hydrogen radical [H•]). The chemical and mechanical effects of acoustic cavitation, particularly inertial cavitation, are commonly leveraged to mediate hydrogel polymerization.

2.2. Acoustic streaming

Acoustic streaming refers to steady or quasi-steady fluid flows induced in a medium due to acoustic energy dissipation or momentum transfer as sound waves propagate.[42] It primarily arises from the effective transfer of acoustic momentum to the fluid medium, driven by boundary layer effects or acoustic attenuation, which induces steady circulatory or directional flows.[43] Acoustic streaming can directly drive fluid motion or exert a drag force on objects suspended within the fluid. It can manifest as "bulk streaming" (macroscopic flow along the sound propagation direction) or "microstreaming" (local vortices or circulatory flows around stably oscillating microbubbles).[44] The shear stress generated by streaming can disrupt the stability of drug carriers, which is applicable in liposome-mediated hydrogel fabrication.[45] Furthermore, by driving macro- or micro-scale flows within precursor solutions, acoustic streaming enhances convection and local mass transfer coefficients, indirectly optimizing fabrication processes such as uniform mixing and degassing.

2.3. Acoustic radiation force

Acoustic radiation force is a steady-state force arising from the transfer of momentum by the acoustic field, primarily acting along the sound propagation direction.[46] When a sound wave encounters an obstacle (e.g., cells, particles, bubbles), scattering, absorption, and reflection occur. This process involves momentum transfer, resulting in a net force on the object.[47] This force can be directly applied to target objects, with its magnitude and direction highly dependent on the object's position within the acoustic field and its acoustic properties.[48]

Gor'kov[49] developed a model to quantify the acoustic radiation force acting on Rayleigh particles at locations where the acoustic field exhibits standing-wave characteristics or, more generally, where the acoustic energy density varies spatially. As expressed in **Equation 2**, the radiation force is obtained from the negative gradient of the Gor'kov potential U.

$$F = -\nabla U \tag{2}$$

The potential U is formulated in terms of the time-averaged acoustic pressure and particle velocity, as given in **Equation 3**:

$$U = \frac{4\pi a^3}{3}\left[\frac{f_1 p^2}{2\rho_0 c_0^2} - \frac{3 f_2 \rho_0 |v|^2}{4}\right] \tag{3}$$

with the prefactor $4\pi a^3/3$ representing the particle volume. The associated scattering coefficients f_1 and f_2, defined in **Equation 4**, depend on the particle and medium properties:

$$f_1 = 1 - \frac{\rho_0 c_0^2}{\rho_p c_p^2}, f_2 = \frac{2(\rho_p - \rho_0)}{2\rho_p + \rho_0} \tag{4}$$

here, ρ_p and c_p denote the particle density and longitudinal sound speed, respectively, and f_1 and f_2 correspond to the monopole and dipole contributions.

This enables direct, non-contact manipulation of the spatial distribution of functional particles (e.g., microparticles, cells) within hydrogel precursors. By engineering the acoustic field (e.g., using standing waves, traveling waves, or complex phased arrays), "acoustic potential wells" can be formed, allowing for precise, label-free capture, translation, rotation, and patterning of particles, cells, or even organisms.[50] This homogenizing capability may play a role in hydrogel preparation.

It is worth noting that the microjets and shear forces generated during inertial cavitation collapse represent transient, extreme-intensity mechanical effects, typically discussed separately from the steady-state acoustic streaming and radiation force, though all belong to the broader category of ultrasound-induced mechanical effects.

2.4. Thermal effect

The thermal effect of ultrasound—a core physical process in its interaction with matter—refers to the conversion of absorbed acoustic energy into heat during propagation.[47,48] Its essence lies in acoustic energy dissipation: the relative displacement and friction of the medium during

alternating compression and rarefaction cycles convert sound energy into heat; periodic compression and expansion under acoustic pressure may also contribute to minor temperature fluctuations.[51,52]

The thermal effect is influenced by ultrasound frequency (high frequencies enable superficial, precise heating, whereas lower frequencies allow deeper, uniform heating), intensity, duty cycle, and focusing. For instance, focused ultrasound (FUS) can concentrate energy into a small focal zone (typically millimeter-scale), enabling localized temperature rises without affecting surrounding materials.[53,54] Based on this thermal effect, ultrasound can directly trigger the solid-to-gel transition of thermosensitive polymers or assist in triggering thermosensitive carriers to release crosslinking agents, thereby initiating gelation. The precise and efficient thermal effects of FUS provide a basis for the feasibility of acoustic-assisted 3D printing and 3D bioprinting.

3. Acoustic-assisted fabrication of hydrogels

Leveraging cavitation, ultrasound can trigger free-radical polymerization in hydrogels. Alternatively, its mechanical and thermal effects can induce polymerization via other mechanisms, often without requiring chemical initiators, yielding hydrogels with uniform structure and complex functionality.[55,56] Beyond direct triggering, ultrasound can indirectly induce polymerization through liposome disruption, enzyme catalysis, or modulation of self-assembly systems. Homogenization is another significant—though often indirect—contribution of ultrasound in hydrogel preparation. Compared to other irradiation methods (e.g., light), the acoustic-assisted process has deeper tissue penetration, offers superior spatiotemporal control, and is considered safer. With advancing ultrasound technology and deeper investigation into influencing factors, future mechanisms may extend beyond those listed, leading to more refined fabrication protocols. This section systematically reviews the mechanisms, roles, and applications of ultrasound in hydrogel fabrication, organized by the underlying principle.

3.1. Cavitation-triggered free-radical polymerization

As described in Section 2.1, inertial cavitation provides strong radical generation that can initiate free-radical polymerization. This section discusses how formulation and acoustic parameters modulate network formation and its properties.[57,58] In the process, viscous media such as glycerol can enhance radical generation while reducing polymer solubility and slowing depolymerization,[59] allowing reaction rates to be tuned by adjusting the glycerol/water ratio.[60] Ultrasound frequency and irradiation time are also critical parameters, modulating the hydrogel's mechanical properties and microstructure, thereby affecting pore size, compressive modulus, degradation behavior, and reaction rate.[60] For instance, Yang *et al.*[61] reported ultrasonic interfacial crosslinking of titanium dioxide-based nanocomposite hydrogels, demonstrating that 80 kHz irradiation produced the densest network and highest mechanical strength (compressive modulus = 80.64 kPa), while 120 kHz yielded optimal sonodynamic activity, achieving a 99.86% bactericidal rate against *Staphylococcus aureus* with good biocompatibility.

Another study noted that different ultrasonic frequencies differentially affect pea protein reorganization and hydration properties, leading to higher structural strength compared to traditionally induced gels.[62] Research on pea protein–psyllium hydrogels showed irradiation duration significantly impacts structure; longer treatment (10 min vs. 5 min) led to decreased encapsulation efficiency, reduced physical stability, antioxidant degradation, and weaker gel strength, though it promoted aggregate dispersion and improved homogeneity.[63] Conversely, extending ultrasound time from 10 to 90 min for nanocellulose hydrogels decreased interfibrillar spacing from 86.81 nm to 6.05 nm, resulting in a denser network and enhanced strength.[64] Increased ultrasonic intensity, time, and power were also reported to improve the fibrillation rate and water retention value of nanofibrillar hydrogels, enhancing network structure and hydrophilicity.[65] Therefore, specific monomer or polymer systems with appropriately selected ultrasonic parameters are key influencing factors in optimizing the acoustic-assisted fabrication process.

Additionally, studies have shown that output power and energy can precisely control reaction rates; higher power accelerates radical generation and shortens gelation time. Adjusting ultrasound dose, frequency, and substrate concentration allows control over crosslink density, swellability, and mechanical properties.[66] At 622 kHz, a 10% hydrophilic polyethylene glycol diacrylate (PEGDA) solution formed a macroscopic gel within 30 s, whereas hydrophobic polyethylene glycol dimethacrylate gelled more slowly, initially forming microgels before producing a macro-gel with lower crosslink density.[67] Using tert-butanol as an •OH radical scavenger, it was confirmed that polymerization was primarily initiated by •OH radicals from water, highlighting monomer hydrophilicity as a key factor.[66]

Solute concentration is another consideration: if too low, radicals self-quench; if too high, increased viscosity impedes cavitation and requires more reaction sites per unit volume. A 5–15% range is often optimal.[66] Solution pH also affects structure. Ching *et al.*[68] reported using

cavitation energy (exceeding hydrogen bond energy) to process microcrystalline cellulose, gradually reducing its size to nanocellulose hydrogel. They investigated the role of acid: without acid, cavitation physically peeled outer layers of fiber bundles, producing high-aspect-ratio, slender nanofibers that formed a stable 3D network at very low gelation concentration. With acid present, acid-catalyzed hydrolysis of glycosidic bonds broke cellulose chains, producing shorter fibers with a lower aspect ratio, leading to a looser hydrogel structure requiring higher fiber concentration for gelation. For greater surface area and adsorption, adding acid during sonication optimizes pore structure; for high-stability nanocellulose hydrogels, acid-free sonication is preferable.[68]

Beyond ultrasonic parameters and solution factors, ambient oxygen threatens radical stability. In radical-dependent syntheses, an inert atmosphere is often crucial. In PEGDA systems, gels formed within 30 s under argon but failed to gel even after 2 h of sonication in oxygen-saturated solutions.[66] Thus, prior understanding necessitates degassing and inert gas reactions in acoustic-assisted hydrogel fabrication. Recent research, however, introduced glycerol as an additive to confer oxygen tolerance. Electron paramagnetic resonance spectroscopy proved glycerol's central role: signals for alkyl radicals (DMPO$^{\bullet}$-R) were far stronger than for hydroxyl radicals (DMPO$^{\bullet}$-OH) in glycerol-containing aqueous solutions under sonication.[69] This indicates that glycerol molecules cleave under cavitation, generating abundant additional, more stable radicals. When the radical concentration at initiation sites is sufficiently high, it can effectively outcompete local oxygen molecules. Even if some radicals are quenched by oxygen, enough remain to initiate monomer polymerization, significantly promoting the reaction. Additionally, glycerol's viscosity slows the oxygen diffusion from the atmosphere into the solution, providing an extended timeframe for radical polymerization.[69]

3.2. Mechanically/thermally triggered polymerization

Based on the mechanical and thermal pathways summarized in Sections 2.3 and 2.4, this section highlights representative hydrogel systems where ultrasound primarily promotes physical crosslinking (mechanical-dominant) or thermosensitive polymerization (thermal-dominant).[70] For example, Norris *et al.*[71] exploited the thermal effect to fabricate collagen–fibronectin composite hydrogels. In a 25 °C water bath at 8.2 W/cm^2, the internal temperature rose from 25 °C to 32.3 °C. This temperature change altered the collagen fibril microstructure, increasing fibril density and inducing polymerization, with temperature-matching experiments confirming the dominance of the thermal effect. Interestingly, another study fabricated collagen hydrogels where the mechanical effect was predominant, as heating alone could not replicate the ultrasonic-induced fibrillar structural changes, confirming that collagen realignment was not thermally driven.[72] This hydrogel served as a skin dressing in genetically diabetic mice, promoting cell infiltration and matrix remodeling in the wound microenvironment.[72]

Another study utilized ultrasonic mechanical forces to prepare alginate/collagen hydrogel microbeads. By disrupting lateral hydrogen bonds between collagen fibers and reorganizing them into nano-dimensions without inhibiting cell proliferation, these beads enabled the culture of uniform 3D tumor spheroids, with potential applications in anticancer drug testing and screening.[73] An ultrasound-assisted directional freezing technique was also proposed to tune the pore size of chitosan-based hydrogels. By using ultrasound's mechanical effect to fragment and control ice crystal growth, hydrogels with finer pores, enhanced mechanical strength, greater intermediate water content, and faster evaporation rates were prepared.[74]

Even when preparing collagen hydrogels, other substances within the system can influence the dominant effects of ultrasound. Jonnalagadda *et al.*[70] reported a system for rapid hydrogel formation via high-intensity FUS (HIFU) in the presence of excess zinc perchlorate salt. Initially, HIFU-induced mechanical stress (as acoustic streaming) disrupted nano-dispersion structures, promoting ligand coordination with Zn^{2+} and inducing gelation. As the gel volume increased, ultrasound absorption caused a bulk temperature rise, further enhancing coordination polymerization and strengthening the gel structure. The study noted that this synergy produced structurally stronger hydrogels than heating alone, and HIFU operating at higher frequencies (>100 kHz) can be focused to a rice-grain-sized volume, offering spatiotemporal controllability.[70] Representative examples of ultrasound-assisted hydrogel formation discussed in Sections 3.1 and 3.2 are summarized in Figure 2.

3.3. Liposome-mediated polymerization

Ultrasound can serve as a remote trigger for polymerization by stimulating responsive carriers to release crosslinking-promoting substances. It can induce transient pore formation in the membranes of carriers such as liposomes, releasing encapsulated ions or enzymes that subsequently initiate hydrogel polymerization. This approach was first demonstrated in 2020, where ultrasound-stimulated calcium-loaded liposomes were used to release Ca^{2+}, which then activated transglutaminase (TGase). TGase catalyzed covalent crosslinking between fibrinogen molecules, forming a hydrogel.[75] By varying ultrasound exposure

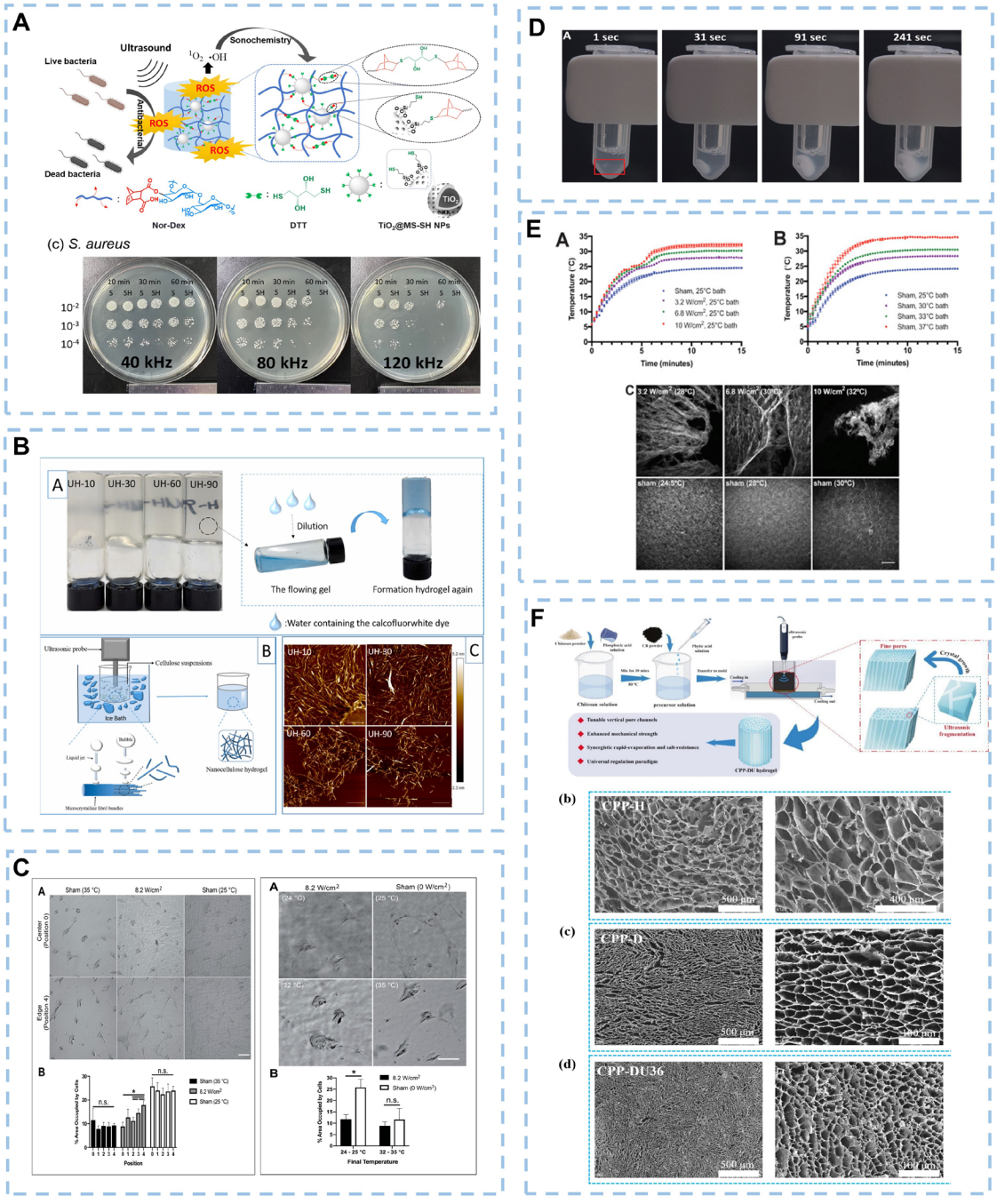

Figure 2. Schematic representation and effects of cavitation, mechanical polymerization, and thermal polymerization for hydrogel preparation. (A) Formation of titanium dioxide@thiol-functionalized mesoporous silica/norfloxacin–dextran (TiO_2@MS–SH/Nor–Dex) nanocomposite hydrogel via ultrasound-triggered thiol–norbornene click reaction and its antibacterial effect. Reprinted with permission from Yang *et al.*[63] Copyright © 2023, The Royal Society of Chemistry. (B) Schematic illustration of ultrasound-assisted preparation of nanocellulose hydrogel and its reversible gel–solid transition (scale bar = 1 μm). Reprinted with permission from Ni *et al.*[64] Copyright © 2022, Elsevier. (C) Influence of ultrasound on the microstructure of collagen–cellulose composite hydrogels (scale bar = 500 μm). Reprinted from Norris *et al.*[71] (D) Rapid hydrogel formation induced by high-intensity focused ultrasound. Reprinted with permission from Jonnalagadda *et al.*[70] Copyright © 2020, Wiley-VCH. (E) Non-thermal effects of ultrasound on collagen assembly and structure. Reprinted with permission from Norris *et al.*[72] Copyright © 2019, Elsevier. (F) Ultrasound-initiated preparation of high-strength hydrogels without initiator under oxygen-tolerant conditions (scale bar = 100 μm; scale bar = 400 μm; scale bar = 500 μm). Reprinted from Cheng *et al.*[69]

time, the amount of released Ca^{2+} could be controlled, linearly regulating the initial reaction rate and catalytic activity of TGase, thereby tuning hydrogelation kinetics and mechanical properties.[75]

Building on this, another study co-encapsulated Ca^{2+} and thrombin within liposomes. Released Ca^{2+} activated TGase, while thrombin catalyzed the hydrolysis of fibrinogen to fibrin monomers. These monomers were then covalently crosslinked by activated TGase, forming a covalently crosslinked fibrin network in situ.[76] This hydrogel promoted microvascular network reconstruction in damaged tissue, largely addressing permeability barrier issues and significantly enhancing microvascular formation.[76] Furthermore, liposome–microbubble complexes can enhance ion release efficiency, further improving gelation rate and control. Microbubbles are often used with FUS systems to precisely trigger gelation at specific locations, suitable for scenarios requiring local repair or drug delivery, offering spatiotemporal control and high penetration depth.[77]

3.4. Enzyme-catalyzed polymerization

The use of TGase represents a cold-set approach for preparing protein-based hydrogels. Compared to thermal setting, TGase better protects bioactive substances and nutrients, is cost-effective, safe, and represents an ideal compound for promoting protein hydrogel polymerization.[78] Ultrasound primarily acts to promote the TGase-catalyzed polymerization reaction in this context. It facilitates protein disaggregation and exposure of active sites, reducing aggregate size, exposing hydrophobic groups, and altering conformation, making proteins more amenable to TGase catalysis. Compared to using TGase alone, the synergistic ultrasonic treatment leads to the formation of denser, more uniform 3D networks with higher mechanical strength and improved water-holding capacity.[79]

Currently, studies have successfully prepared egg white–bovine gelatin composite hydrogels[80] and pea protein hydrogels[81] via high-intensity ultrasonic pretreatment followed by TGase-catalyzed polymerization, both exhibiting promising properties for food and pharmaceutical applications. Different ultrasonic durations also exert distinct effects: a 10-min treatment formed hydrogels with a uniform honeycomb structure, significantly improved gel strength, water-holding capacity, and mechanical properties, whereas a 1-min treatment yielded hydrogels with high viscosity and good support, self-repair, and printability.[81]

3.5. Self-assembly systems for polymerization

The primary mechanism for ultrasound-triggered hydrogel formation based on self-assembly systems involves sonication, disrupting intramolecular hydrogen bonds, converting molecules into an activated state primed for intermolecular interactions. Subsequently, via non-covalent interactions, such as intermolecular hydrogen bonding and π–π stacking, molecules self-assemble into a 3D crosslinked network.[82] Utilizing this principle, Chen *et al.*[83] developed a hydrogel using a reduced-end free glucose aminobarbiturate as a gelator. Ultrasound triggered its self-assembly into a 3D network while enabling the in situ synthesis and stable encapsulation of silver nanoparticles without additional reductants or stabilizers. The composite demonstrated good antibacterial activity against both Gram-positive and Gram-negative bacteria, highlighting its potential as a broad-spectrum, antibiotic-free antimicrobial hydrogel containing silver nanoparticles.[84]

Such systems also show promise in drug delivery. An ultrasound-induced aspartic acid derivative supramolecular hydrogel could load 500 mg of the drug niclosamide per mL. Niclosamide release was faster in the first 24 h, then slowed, sustaining release for 15–22 days, demonstrating excellent sustained-release capability alongside good mechanical properties and biocompatibility.[85] Another study developed a novel L-lysine–based low-molecular-weight hydrogelator suitable as a cell scaffold for tissue engineering. It self-assembles via hydrogen bonding and π–π stacking into fibers that further crosslink into a 3D network. Ultrasonic treatment dramatically accelerated gelation from 3 h to 30 s. Microscopy revealed that untreated samples exhibited short, irregular fibers, while sonicated samples exhibited longer, more uniform fibers with consistent diameters, promoting ordered assembly and yielding hydrogels with better mechanical properties.[86] Fibroblasts cultured on this hydrogel exhibited good adhesion, spreading, migration, and proliferation.[86]

Additionally, ultrasound can convert precipitates into hydrogels via self-assembly. For instance, cyclo(L-Tyr–L-Lys) typically precipitates in water but forms a hydrogel under ultrasonic assistance. Sonication promotes more orderly molecular aggregation, inducing nucleation and self-assembly into a fibrous network instead of precipitation.[87]

Ultrasound-triggered hydrogel fabrication based on self-assembled systems can also be used to prepare hydrogels with specific structures. Ma *et al.*[88] first

developed naphthalimide derivative-based self-assembled nanotube structures that undergo instantaneous transition from suspension to hydrogel upon ultrasound triggering, without heating or other aids. The nanotubes have a hydrophilic exterior but hydrophobic inner cavities inaccessible to water at rest. Ultrasound generates powerful physical forces that "inject" water molecules into the cavities, triggering hydrogel formation. The gelation process and final morphology can be tuned by ultrasonic parameters, showing stimulus responsiveness, with different morphologies also forming at different pH values. The hydrogels exhibit a good in situ drug-loading capacity.[88] Ultrasonic duration also affects self-assembled structure: short durations (<1 min) yield fine fibers coexisting with crystals, while longer durations (>5 min) promote fiber growth and crystal disappearance.[89] Although ultrasound-induced hydrogels have higher mechanical strength, when dealing with crystalline materials, they may be less stable and rapidly revert to crystalline precipitates.[89]

3.6. Homogenization effects in polymerization

Beyond directly causing polymerization, the homogenization effect arising from cavitation and mechanical effects plays a crucial, albeit indirect, role in hydrogel preparation. Ultrasound disrupts intermolecular forces between particles, preventing agglomeration, improving dispersity, reducing particle size, and ensuring more uniform distribution, thereby optimizing the final hydrogel structure and properties.[90] Qu *et al.*[91] employed ultrasonic homogenization to prepare a thermoresponsive lignin-reinforced poly(ionic liquid) double-network hydrogel, uniformly dispersing lignin and ionic liquid in water to promote monomer mixing and polymerization, contributing to a uniform polymer network and enhancing mechanical and conductive properties. This hydrogel was used for human motion detection, body temperature monitoring, and as a flexible touch panel for letter recognition and Braille input.[91]

Another study used ultrasonic homogenization to successfully embed nanobentonite as a filler and crosslinker into a polymer network, improving hydrogel structure and adsorption performance.[92] The homogenization effect not only disperses substances but can also disperse macromolecules and uncoil their structures, increasing surface binding sites. Moderate ultrasonic power (e.g., 60%) can form the most uniform and dense network, while excessive power (e.g., 80%) may break molecular chains, causing irregular aggregation.[93] Therefore, ultrasonic homogenization serves as an efficient physical pretreatment method, providing dispersion to prevent particle agglomeration,[94] while also modulating hydrogel structure, properties, and reaction rates.[95]

3.7. Other mechanisms

Kang *et al.*[96] utilized surface acoustic wave (SAW)-induced steady flow vortices for non-contact, spatiotemporally precise control over hydrogel polymerization. SAW generated local fluid vortices that captured hydrogel microparticles in solution. During polyacrylamide hydrogel formation, vortex positions developed denser PAAM polymer networks, while other regions formed coarser networks. SAW propagation creates a unidirectional fluid jet in the solution and a reverse flow at the polydimethylsiloxane (PDMS) interface, with their interaction generating flow vortices that capture and concentrate microparticles at vortex centers. During polymerization, polymer chains and microparticles are transported to vortex centers, where concentrated particles interconnect, forming high-density gel networks; regions between vortices form relatively sparse networks. Thus, SAW creates structural and property gradients (from center to edge) within a single hydrogel. This gradient hydrogel was used as a cell culture substrate, successfully regulating cell morphology (NIH-3T3 fibroblasts and human adipose-derived stem cells exhibited position-dependent morphologies: rounded in central/stiffer regions and elongated in peripheral/softer regions), demonstrating potential for interface tissue engineering to simulate soft-hard tissue interfaces and for applications in soft robotics and biosensors.

Another study utilized ultrasound energy to drive the breakage and reformation of coordination bonds, facilitating a chemical transformation from a kinetically stable amine complex to a thermodynamically more stable terpyridine complex.[97] Ultrasound has also been used not for synthesis but to modulate local mechanical properties of pre-formed hydrogels. FUS triggered acoustic droplet vaporization, converting emulsion droplets into bubbles whose formation and growth radially compressed the surrounding fibrin matrix, increasing local density and stiffness. By controlling the focus location and parameters, regions with different stiffness could be precisely generated within the hydrogel.[98]

Figure 3 illustrates the overview of representative "indirect" mechanisms that enable ultrasound-responsive gelation beyond direct radical/thermal routes.

3.8. Applications of acoustically fabricated hydrogels

In biomedical applications, ultrasound-fabricated hydrogels offer unique advantages: rapid synthesis, more uniform 3D structure, and commonly enable polymerization in the absence of chemical initiators.[99,100] Ebrahimi *et al.*[55] synthesized acrylate hydrogels in water/glycerol media under ultrasonic irradiation, demonstrating

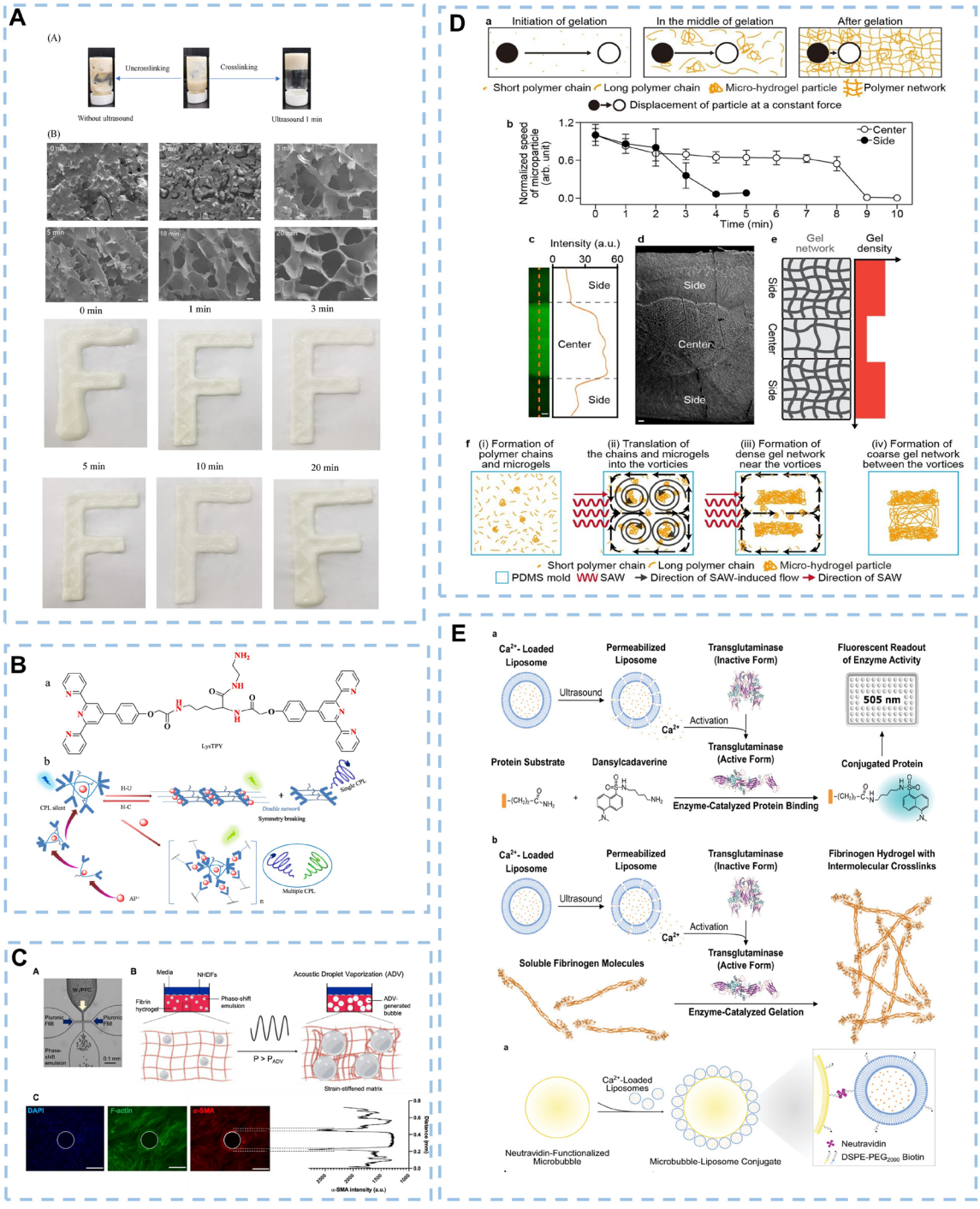

Figure 3. Other mechanisms and effects of ultrasound in hydrogel preparation. (A) Ultrasound-triggered enzymatic gelation (scale bar: 50 μm). Reprinted with permission from Wang *et al.*[79] Copyright © 2023, Wiley-VCH. (B) Schematic diagram of ultrasonic preparation of lysine–terpyridine conjugate (LysTPY). Reprinted with permission from Guo *et al.*[97] Copyright © 2021, American Chemical Society. (C) Acoustically responsive scaffold: hydrogel matrix embedded with phase-transition emulsion droplets enabling local modulation of stiffness via focused ultrasound (scale bar: 200 μm). Reprinted with permission from Farrell *et al.*[98] Copyright © 2022, Elsevier. (D) Fabrication of hydrogels using surface acoustic waves. Reprinted with permission from Kang *et al.*[96] Copyright © 2024, Elsevier. (E) Schematic diagram of ultrasound-induced liposome disruption triggering gelation. Reprinted from Nele *et al.*[75]

significantly faster synthesis (a few minutes) compared to non-sonicated controls, with more uniform microstructure and higher swellability. pH-dependent drug release studies (pH 5–9) revealed high pH sensitivity and reversible pH-responsive swelling/deswelling, indicating potential as tissue engineering materials and intelligent drug delivery systems capable of site-specific release in the gastrointestinal tract.

Another study used acoustic cavitation to synthesize sodium lignosulfonate-grafted poly(acrylic acid-co-vinylpyrrolidone) hydrogels loaded with amoxicillin. The hydrogel better preserved drug activity, achieved high loading, and showed clear pH-responsive release (51.5% cumulative release in simulated gastric fluid vs. 84.5% in simulated intestinal fluid over 24 h), suitable for oral drug delivery with diffusion-controlled release for sustained action and reduced side effects.[101] A phenylalanine-derived hydrogel fabricated via acoustic cavitation was used to encapsulate anticancer drugs—5-fluorouracil and methotrexate. The ultrasound-induced hydrogel exhibited higher network density and mechanical stability, with smoother and more uniform fiber surfaces, resulting in higher drug encapsulation efficiencies (83% for 5-fluorouracil and 81% for methotrexate). It maintained drug release behavior in acidic environments, supporting its use as a tumor microenvironment-responsive delivery platform, and the 3-(4,5-dimethylthiazol-2-yl)-2,5-diphenyltetrazolium bromide assay (also known as MTT assay) confirmed good biosafety.[102]

Ultrasound can also trigger *in vivo* hydrogel formation. Zhu *et al.*[103] developed an ultrasound-triggered in situ hydrogel system (2,2'-azobis[2-(2-imidazolin-2-yl) propane] dihydrochloride/PEGDA/doxorubicin [DOX]/catalase-chlorin e6). Under ultrasound, 2,2'-azobis[2-(2-imidazolin-2-yl) propane] dihydrochloride decomposed into alkyl radicals, initiating PEGDA polymerization to form a hydrogel that localized catalase-chlorin e6 and DOX at the tumor site. Long-term hydrogel retention allowed catalase to continuously decompose endogenous hydrogen peroxide into oxygen, alleviating hypoxia and enhancing photodynamic therapy, while DOX was slowly released for combined chemo-photodynamic therapy. *In vivo* experiments showed significant synergistic antitumor efficacy with a single injection and no obvious side effects.

Beyond drug delivery, cavitation-fabricated hydrogels show promising potential in flexible sensors and tissue engineering.[57,99] Li *et al.*[104] synthesized polyacrylamide–sodium alginate double-network hydrogels using MXene (titanium carbide) as a reductant and potassium persulfate as an oxidant. Acoustic cavitation decomposed MXene and potassium persulfate to generate radicals, initiating polymerization and yielding highly tough and conductive hydrogels. As a strain sensor attached to a finger, it monitored bending motions via resistance changes. It also showed potential for electrocardiogram monitoring as hydrogel electrodes, demonstrating high stability and reproducibility for real-time cardiac health monitoring.[104]

In tissue engineering, ultrasound via cavitation causes molecular collisions, generating local high pressure and temperature, which disrupt protein non-covalent bonds, partially unfolding proteins to expose hydrophobic groups and disulfide bonds, increasing crosslink density[58] and promoting protein aggregation. This was used to induce the solid-to-gel transition of sericin protein.[105] Cell experiments validated its potential as a cell carrier/culture platform: mouse fibroblasts on the hydrogel surface proliferated, adhered, migrated, and survived up to 42 days, with adhesion rates and viability comparable to those on conventional culture plates. Horseradish peroxidase encapsulation demonstrated sustained release capability, establishing sericin hydrogel as a versatile platform for cell culture and drug release.[105]

Beyond biomedical applications, cavitation-fabricated hydrogels are applied in food and environmental sectors.[106,107] Their efficiency, green nature, and precision offer broad prospects in food (e.g., encapsulating heat-sensitive bioactive components like probiotics or liposoluble vitamins[108]) or as food additives.[58] In environmental remediation, an ultrasound-assisted in situ free-radical copolymerization method was used to synthesize a magnetic double-network nanocomposite hydrogel for the adsorption of organic pollutants, especially phenols, with recyclability and regeneration capabilities.[109]

Ultrasound improved the adsorption capacity and mechanical properties. The hydrogel also showed pH responsiveness, adsorbing phenol optimally at pH 9 and 4-nitrophenol at neutral pH, allowing performance adjustment based on water acidity.[109] Another approach combined hydrogel preparation with hydrodynamic cavitation to enhance dye removal efficiency, offering a new strategy for wastewater treatment intensification.[110] An ultrasound-assisted in situ free-radical polymerization method was used to synthesize poly(acrylic acid)/bentonite/iron–cobalt nanocomposite hybrid hydrogels for the adsorption of the cationic dye crystal violet. High shear gradients from cavitation helped control molecular weight and promoted precursor (e.g., iron[II] chloride, cobalt[II] chloride) dispersion within bentonite interlayers.[111] This hydrogel exhibited pH responsiveness (optimal adsorption at pH 11 due to carboxyl group dissociation, enhancing electrostatic attraction with cationic dyes, decreasing in acid) and temperature responsiveness (increased

adsorption with temperature up to 35 °C, as heating relaxes the polymer network), making it suitable for treating dye wastewater from textiles, printing, and cosmetics.[111]

Another study used ultrasound to prepare poly(acrylic acid)–kaolin hybrid hydrogels for adsorbing cationic dye Brilliant Green, retaining similar advantages, while kaolin addition enhanced mechanical strength and water retention, suggesting uses in soil amendment and slow-release fertilizer carriers.[112] Such hydrogels also adsorb metal ions. Wang *et al.*[113] synthesized a hydrogel via ultrasound-assisted free-radical polymerization that effectively adsorbed Co^{2+} ions, outperforming many traditional adsorbents for cobalt-containing wastewater from electroplating, alloy, and catalyst industries. Another study developed a sodium lignosulfonate-based superabsorbent hydrogel via an ultrasound-assisted method for effective Ni^{2+} ion adsorption, with potential application in treating nickel-containing wastewater from electroplating and battery manufacturing, and with additional capacity to adsorb other metal ions.[114]

Application-oriented examples of acoustically fabricated hydrogels are illustrated in Figure 4, spanning biosensing, drug delivery, in situ tumor therapy, and environmental remediation. The characteristics of different mechanisms for ultrasound-induced hydrogel formation are summarized in Table 1.

4. Acoustic-assisted 3D printing and 3D bioprinting

As understanding of ultrasound-triggered hydrogel fabrication mechanisms, materials, conditions, and applications matured, acoustic-assisted 3D printing and 3D bioprinting have attracted increasing attention. 3D printing and 3D bioprinting hold immense potential in tissue engineering and personalized medicine for constructing specific tissue substitutes and complex scaffolds for repair.[115] However, its clinical translation is limited by reliance on invasive surgical implantation, conflicting with the minimally invasive paradigm.[116] Acoustic-assisted 3D printing and 3D bioprinting, leveraging ultrasound's deep tissue penetration, potential for high precision, biocompatibility, and real-time imaging capability, offer a promising new pathway by enabling in situ printing at defect sites—an advantage lacking in traditional light-based or extrusion techniques.[21,117,118] Several researchers have explored the application of ultrasound mechanisms—cavitation, mechanical effects, thermal effects, and liposome-mediated polymerization—in acoustic-assisted 3D printing and 3D bioprinting.

4.1. Three-dimensional printing

Debbi *et al.*[119] utilized inertial cavitation to locally generate free radicals, polymerizing PEGDA and poly(vinyl alcohol) methacrylate. Their results showed complete polymerization of 10% PEGDA or poly(vinyl alcohol) methacrylate solutions under 37 kHz or 1 MHz ultrasound. A five-second exposure at 2.2 W cm^{-2} achieved complete polymerization, while lower intensities yielded the same results with prolonged exposure time, aligning with prior literature.[66] They further explored cell encapsulation within such ultrasonically polymerized hydrogels. Due to radical cytotoxicity,[120] cells required additional protection via alginate or fibrin encapsulation, boosting viability from 60% to 89% while preserving function.[119] Finally, by increasing the acoustic ink's viscosity to enhance localized cavitation energy release, reduce radical diffusion, and accelerate polymerization decay, they achieved millimeter-scale acoustic-assisted 3D printing. Combined with cell encapsulation results, they demonstrated the potential for cavitation-based acoustic-assisted 3D bioprinting,[119] though limitations include low resolution, difficulty printing complex 3D structures, and inherent radical cytotoxicity.[33]

The extreme temperatures, pressures, and heating/cooling rates induced by cavitation have been exploited for thermal polymerization in acoustic-assisted 3D printing.[121-123] Habibi *et al.*[124] applied FUS within a chamber filled with a thermally curable polymer (primarily PDMS). By leveraging the rapid heating/cooling at the FUS focus, they achieved 3D printing of PDMS, terming the method direct sound printing (DSP). The printing process involved moving the FUS focus point-by-point along a preset path within the chamber, depositing cured voxels onto a platform or previously cured voxels, achieving approximately 280 μm resolution, albeit with severely limited speed due to point-by-point writing.[124] To improve printing speed, they subsequently proposed holographic DSP (HDSP).[125] HDSP uses acoustic holography to generate a sound pressure pattern across an entire image plane, inducing polymerization simultaneously across a cross-section rather than point-by-point. While a single hologram can print simple two-dimensional shapes, moving the build platform with a robotic arm along a 3D path enables more complex structures.[125] Leveraging FUS penetration, both DSP and HDSP can achieve remote, deep-tissue printing (e.g., through 15 mm-thick biological tissue). However, the extreme temperatures from inertial cavitation may limit their use with cell-laden bioinks. Furthermore, the method has been primarily demonstrated with PDMS; other

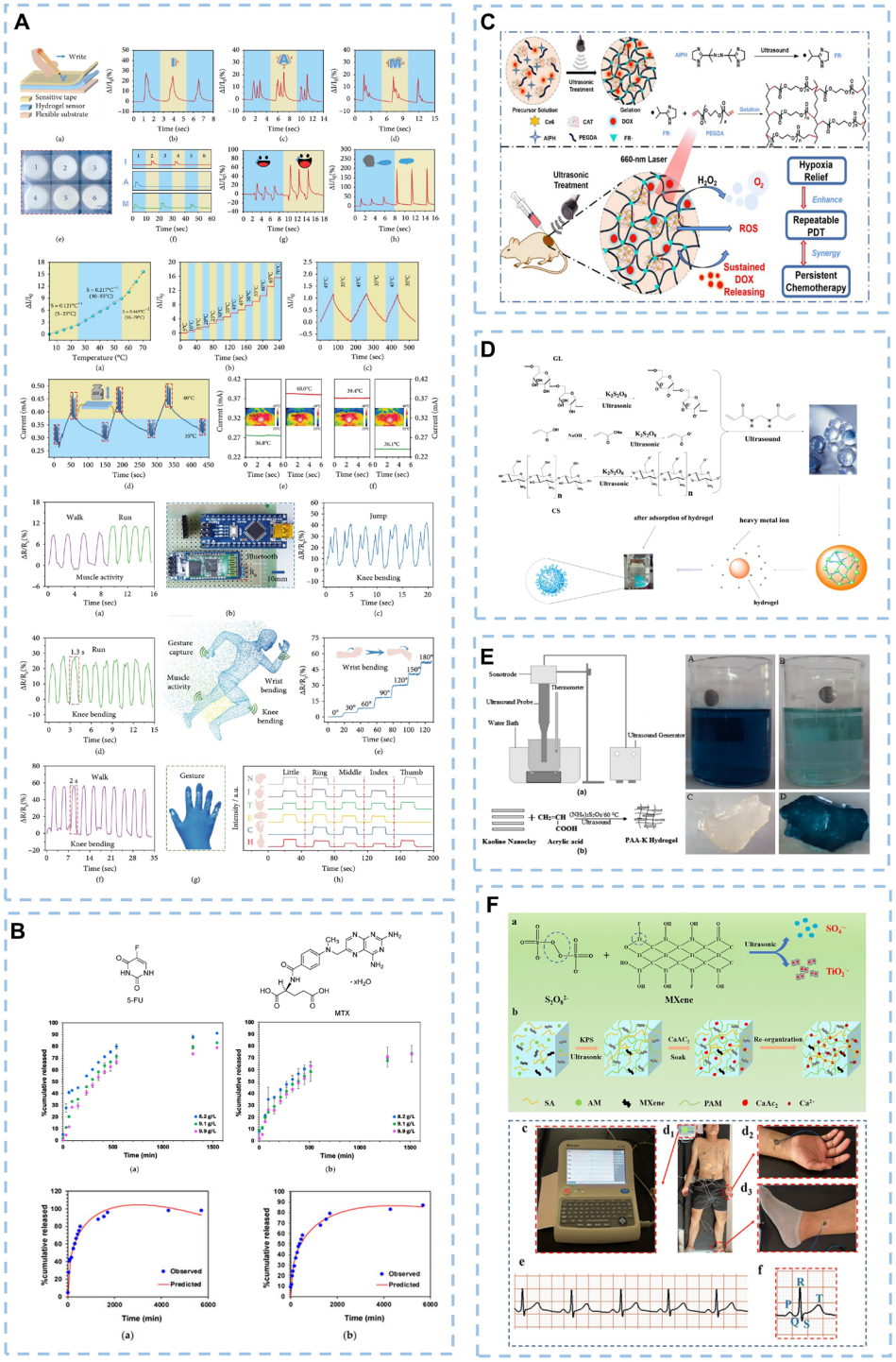

Figure 4. Biological applications of ultrasound-prepared hydrogels. (A) Ultrasound-assisted synthesis of lignin-reinforced poly(ionic liquid) hydrogels for biosensor applications. Reprinted from Qu *et al.*[91] (B) Ultrasound-fabricated phenylalanine-derived hydrogel as an efficient drug delivery platform. Reprinted from Buxaderas *et al.*[102] (C) In situ synthesis of hydrogel for antitumor therapy. Reprinted with permission from Zhu *et al.*[103] Copyright © 2025, Wiley-VCH. (D) Ultrasound-assisted synthesis of gelatin (GL)/chitosan (CS) hydrogel for the adsorption of heavy metals in the environment. Reprinted with permission from Jiang *et al.*[107] Copyright © 2019, Elsevier. (E) Ultrasound-synthesized poly(acrylic acid) hydrogel for wastewater treatment. Reprinted with permission from Shirsath *et al.*[112] Copyright © 2013, Elsevier. (F) Mechanism of ultrasound-induced redox reaction between MXene and potassium persulfate and its biosensing application. Reprinted with permission from Li *et al.*[104] Copyright © 2023, The Royal Society of Chemistry.

Table 1. Comparative summary of mechanisms for ultrasound-induced hydrogel formation

Mechanisms	Gelation time	Cytocompatibility	Applicable materials	References
Cavitation-triggered free-radical polymerization	Ranging from tens of seconds to tens of minutes	Mouse embryo fibroblasts	PEGDA, PEGDMA, nanocellulose hydrogels, microcrystalline cellulose, and Pluronic F127	61,64,66
Mechanically/thermally triggered polymerization	Varying from minutes to tens of minutes	Fibronectin-null mouse embryonic fibroblasts	Type I rat tail collagen, ECM, alginate/collagen, and chitosan	70-74
Liposome-mediated polymerization	30 s	Human umbilical cord blood endothelial cells	Collagen, fibrin, agarose, and alginate	75-77
Enzyme-catalyzed polymerization	1 min	Excellent	Pea protein, egg white, protein, and gelatin	79,80
Self-assembly systems for polymerization	Within a timeframe spanning tens of seconds to tens of minutes	HeLa cells, mouse NIH 3T3 fibroblasts	L-lysine, aspartic acid derivative, and naphthalimide derivative	83,85,88
Homogenization effects in polymerization	Functioning as an adjunct to other mechanisms	-	Thermoresponsive, polyacrylamide/bentonite hydrogel, hawthorn pectin, and soybean protein isolate	91-93
Surface acoustic wave	Spatiotemporally modulated	Fibroblast cells, adipose-derived stem cells	Polyacrylamide hydrogel	96
Acoustically responsive scaffold	Spatiotemporally modulated (focused ultrasound)	Human dermal fibroblasts	Fibrinogen	98

Abbreviations: ECM: Extracellular matrix; PEGDA: Polyethylene glycol diacrylate; PEGDMA: Polyethylene glycol dimethacrylate.

thermally curable materials require further exploration, and printing capability for complex 3D structures requires further development.

Another study successfully printed three types of thermosets with different polymerization mechanisms using combined thermal and cavitation effects of ultrasound: PDMS (via hydrosilylation), acrylates (via free-radical polymerization), and epoxy resins (via cationic ring-opening polymerization).[126] The technology enabled continuous fabrication of homogeneous and heterogeneous thermosets, including functionally graded composites. By directly inserting an ultrasonic transducer into the liquid thermoset or integrating it with a nozzle, rapid in situ gelation occurred at the transducer's output face. Integrated robotic arms enabled 360° omnidirectional manufacturing, allowing rapid printing of structures like vertical and lateral spirals with spatiotemporal control.

However, resolution is influenced by printing parameters and transducer diameter, currently lacking micrometer precision. Additionally, the thermosets have limited potential for cell-laden bioprinting.[126] Another study used FUS for 3D printing of thermally curable acrylate resins.[127] The resin (PEGDA and 2-hydroxyethyl acrylate) was infused into an opaque foam scaffold. Moving the FUS focus within the foam triggered resin curing, enabling support-free, layerless, freeform 3D fabrication. The modulus could be tuned from hard to soft by adjusting PEGDA/2-hydroxyethyl acrylate ratio. The foam scaffold mitigated acoustic streaming in low-viscosity ink, improving precision, and provided support for curing parts, enabling fabrication anywhere within the foam. However, resolution was also non-microscale (around 6

mm minimum feature size), and reliance on a sacrificial foam scaffold poses practical limitations for removal and structural integrity.[127] Figure 5 summarizes representative acoustically assisted 3D printing strategies.

4.2. Three-dimensional bioprinting

While the pioneering studies discussed in Section 4.1 achieved high-precision, non-contact, controlled 3D printing, their application in bioprinting remains constrained by cell damage risks from cavitation-generated radicals, thermal effects, and bioink biocompatibility limitations.

Kuang *et al.*[128] developed a self-enhancing, phase-transition, ultrasound-responsive bioink for FUS-guided volumetric bioprinting. The bioink comprised PEGDA or other vinyl oligomers (e.g., gelatin methacryloyl) as the base, agarose microparticles as a rheological modifier, poly(N-isopropylacrylamide) (PNIPAm) as a self-enhancing acoustic absorber, and ammonium persulfate as a thermal initiator. PNIPAm undergoes a coil-to-globule phase transition upon heating, significantly increasing viscosity.[129] The ink also exhibited strong shear-thinning behavior. This bioink addressed the conflict between acoustic penetration depth and streaming: shear-thinning promoted deep penetration under high-frequency sound, while phase-transition–induced viscosity increase markedly reduced streaming, enhanced acoustic absorption, and enabled rapid, localized heating, significantly improving printing precision.

As a direct result of self-enhanced attenuation and viscosity, the ink showed rapid, self-enhanced heating: within seconds of FUS exposure, the focal zone temperature rose rapidly to 60–80 °C. Through this thermal effect, the thermal initiator ammonium persulfate generated radicals to trigger vinyl oligomer polymerization, leading to rapid bioink gelation.[130] This approach enabled direct, contact-free volumetric printing without a build platform, advantageous for *in vivo* applications. Both PEGDA-based and gelatin methacryloyl-based acoustic inks using NIH/3T3 fibroblasts showed minimal to no cytotoxicity.[131,132] Printing precision reached the sub-millimeter scale, with the capability for centimeter-sized constructs. The use of confocal dual transducers could further improve resolution and speed while minimizing potential tissue side effects.

The study validated the potential of acoustic-assisted 3D printing for deep-tissue engineering, demonstrating penetration printing in *ex vivo* tissues and non-contact ink solidification for left atrial appendage occlusion in an *ex vivo* goat heart. Leveraging ink versatility, they also formulated a PEGDA/agarose/PNIPAm nanocomposite ink with 5 wt% hydroxyapatite nanoparticles for printing bone repair scaffolds and created a doxorubicin-loaded PEGDA/agarose/PNIPAm hydrogel for sustained targeted chemotherapy in liver tumors in situ. Despite this breakthrough, potential cytotoxicity from high polymerization temperatures remains a concern.[128]

A recent study addressed the biosafety issue of thermal polymerization during printing. Davoodi *et al.*[133] developed an *in vivo* acoustic printing platform based on low-temperature–sensitive liposomes (LTSLs). In this technology, LTSLs encapsulate crosslinkers and are designed to release their payload at a temperature slightly above body temperature upon FUS exposure. This released crosslinker can then trigger gelation via various mechanisms (e.g., ionic crosslinking, oxidative crosslinking, radical polymerization) in the base material. Incorporating small amounts of lysolipid and PEGylated lipid into the LTSL formulation creates grain boundary defects in the lipid bilayer, which rapidly expand upon heating,[134,135] enabling controllable payload release while minimizing premature leakage at physiological temperatures, ensuring acoustic responsiveness and printing precision. Using 8.75 MHz FUS at a printing speed of 40 mm s^{-1}, the study achieved unprecedented 150 μm line-width resolution, maintained at sub-millimeter scale even through 15 mm-thick porcine muscle tissue.[133]

Due to the biocompatibility of both base materials and LTSLs and a crosslinking temperature controlled below 42 °C, the technology showed good cytocompatibility. The platform is highly versatile, enabling the printing of various functional biomaterials. For example, mixing ultrasound contrast-agent microcapsules into the bioink allowed real-time monitoring, precise focal positioning, and in situ crosslinking verification via capsule rupture during printing. Adding conductive additives (e.g., carbon nanotubes, silver nanowires, MXene) to an alginate–LTSL system enabled fabrication of personalized bioelectronic devices for health monitoring.[136] Mixing drugs into the bioink allowed sustained local drug delivery post-printing. Formulating tissue-adhesive bioinks enabled non-invasive wound closure.

The study performed the first *in vivo* printing assessments in live animals: for instance, precisely printing a gel construct targeting bladder cancer tissue within a mouse bladder, monitored via ultrasound imaging, enabling surgery-level targeted therapy while minimizing systemic toxicity. Printing gel lines in deep muscle tissue of a rabbit model further validated the platform's potential in tissue engineering. Post-implantation analysis confirmed high biocompatibility and structural/functional integrity over time, validating platform efficacy.[133] The key innovation

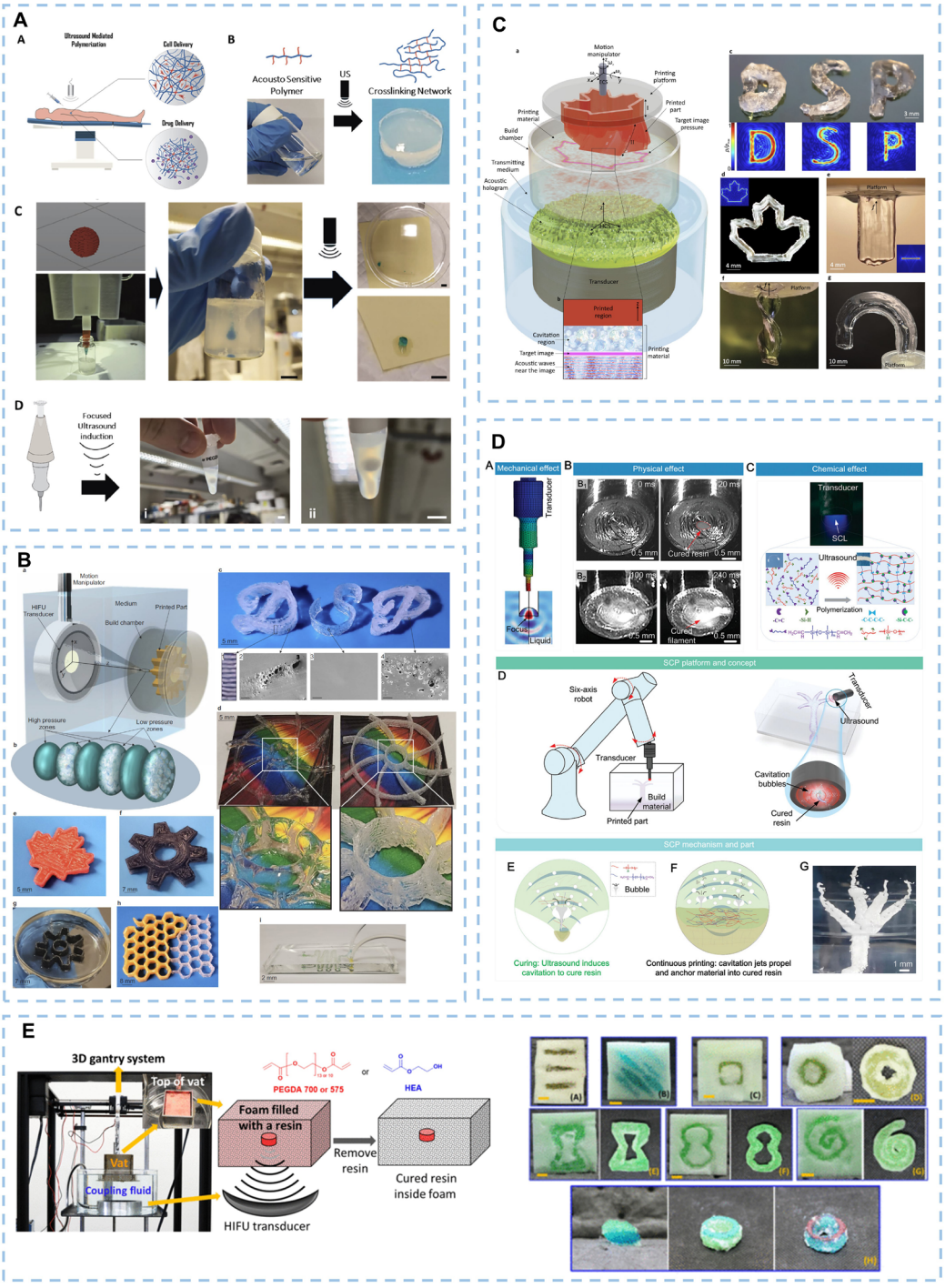

Figure 5. Acoustic-assisted 3D printing.(A) Fabrication and 3D printing of hydrogels (PEGDA or PVA-MA) via acoustic cavitation-triggered free-radical polymerization. Reprinted with permission from Debbi *et al.*[119] Copyright © 2024, Wiley-VCH. (B) Schematic diagram and photograph of the voxel-by-voxel printing process in DSP. Reprinted with permission from Habibi *et al.*[124] Copyright © 2022, Nature Portfolio. (C) Schematic diagram and image of the printing process in HDSP based on acoustic holography. Reprinted from Derayatifar et al.[125] (D) Concept, working principle, and image of continuous thermal polymerization printing based on an integrated ultrasonic transducer. Reprinted with permission from Yao *et al.*[126] Copyright © 2024, Wiley-VCH. (E) Working principle and photograph of 3D printing of thermally curable acrylate resins using FUS. Reprinted from Lee *et al.*[127]
Abbreviations: 3D: Three-dimensional; DSP: Direct sound printing; FUS: Focused ultrasound; HDSP: Holographic direct sound printing; PEGDA: Polyethylene glycol diacrylate; PVA-MA: Poly(vinyl alcohol) methacrylate.

lies in a leap in temperature safety: by using LTSLs to encapsulate crosslinkers, the triggering temperature was successfully reduced from 60–80 °C in traditional acoustic thermal polymerization to 41.7 °C, significantly lowering thermal damage risk.[137]

Figure 6 presents two representative deep-tissue acoustic bioprinting paradigms: self-enhancing sono-inks for volumetric printing and low-temperature, as well as liposome-mediated *in vivo* sound printing. The characteristics of representative studies of acoustic-assisted 3D printing and 3D bioprinting are summarized in Table 2.

Table 2. Characteristics of representative studies on acoustic-assisted three-dimensional printing/bioprinting

Technique	Resolution	Scalability/ throughput	Energy requirements	Acoustic field design	Process parameters	Equipment
DSP[124]	450 μm lines with 25 μm gap at 2.15 MHz; 280 μm lines with 186 μm gap at 2.4 MHz	Printable materials include heat-curing PDMS; remote-distance printing through opaque obstacles; *ex vivo* deep printing; for example: 15 mm tissue + 18 mm PDMS (total 33 mm)	Printing as low as 20 W; some at 20 W or 40 W; 210 W for visualization; printing intensity ~100 W/cm^2 at 20 W; printing pressure <2 MPa; simulated max 3 MPa at platform in a setup	2.15 MHz and 2.4 MHz; monolithic spherically focused transducer; single-element focus	PDMS Sylgard 184; 10:1 porous, ≥13:1 transparent (13:1 borderline)	Build volume: limited by the chamber and motion range
HDSP[125]	Diffraction-limited ~λ/2 in high-pressure areas, but practical image thickness ~λ; hologram printed by SLA with nominal 125 μm (~λw/5 in water at 2.2 MHz); confocal scan shows <30% area deviates >150 μm, inducing unwanted lobes	Speed: 30–90 s (HDSP) vs. 4–13 min (DSP) for comparable wall; remote distance printing through opaque media/ tissue	Acoustic power 5–25 W depending on complexity (to reach ~2 MPa threshold); DSP: 1.18 W, ~12.56 min, ~889 J deposited; ~7,536 J system input; HDSP: 23.18 W, ~0.5 min, ~695 J deposited; ~2,790 J system input	Frequency: 1.86–2.85 MHz; amplitude via power and ~2 MPa threshold; too high power degrades uniformity via streaming; single-element flat transducer + passive hologram	PDMS (following DSP paradigm)	Build volume limited by hologram/ transducer aperture and robot workspace
HIFU curing inside foams[127]	Smallest cured cylinder diameter: ~6 mm at 2 s; ~19 mm at 10 s; focal size: 1.76 mm (width) × 12.91 mm (length)	Free-form curing inside opaque open-cell foam (not layer-by-layer); multi-material via resin exchange	Frequency: 916 kHz, duty cycle 100%, power 50–250 W, thermal imaging: >80 °C in foam within 5 s, bulk resin max ~32 °C due to streaming	Frequency: 916 kHz; single-element HIFU; geometric focus: 63.2 mm; focal depth: 51.6 mm	Open-cell PU foam + thermally curable acrylate resins (PEGDA or HEA formulations); exposure 10–15 s for static and toolpaths retraced 5–7×	Build volume bounded by foam/vat geometry and reachable focal region

(*cont'd...*)

Table 2. (*Continued*)

Technique	Resolution	Scalability/ throughput	Energy requirements	Acoustic field design	Process parameters	Equipment
SCP[126]	Minimum feature 200 μm; with mask templates <100 μm; resolution mainly determined by transducer diameter	Multiscale via transducer-size and pressure control; six-axis robot enables omnidirectional unsupported printing; multi-material thermosets and composites	Controller output 0–100 W with auto frequency tracking; sound pressure: 1.1–3.0 MPa; multi-material examples ~2.95–4.33 MPa	Frequency: 40–50 kHz; Langevin longitudinal transducer with concave end-face focusing; single emitter; shaped by end geometry; focal size at 46 kHz reported (e.g., 3/1.5/1 mm)	PDMS (10:1), epoxy, acrylate or composites; 30–60 °C	Build volume limited by robot workspace
DAVP[128]	Acoustic-pressure FWHM of focal zone: 0.3–0.7 mm; for example, focal zone 0.45 mm at 3.41 MHz; in-plane curing size improved from 7.6 to 1.6 mm when the scan speed was 0.4 to 0.8 mm/s. Axial curing size: 5.0–9.9 mm	No build platform; volumetric deposition but still scanned-focus writing; through-tissue up to ~17 mm with layered phantom example (skin/ fat/muscle 3/5/7 mm)	Input power: <100 W; peak pressure: 35–55 MPa; duty cycle: 90%	Frequency: 2.05, 3.41, and 6.86 MHz; amplitude expressed as peak acoustic pressure (tens of MPa); array geometry: single focus; focal length up to ~64 mm; depth of focus: 5.58 mm (2.05 MHz) vs. 1.69 mm (6.86 MHz)	Materials: PEGDA + agar microparticles + PNIPAm absorber + APS initiator; example ratio: 20/10/3 wt%; curing threshold Tc = 67 °C (0.5 wt% APS), reducible to 62 °C with higher APS	Build volume: ink tank thickness example 10 mm for characterization
DISP[133]	Reported resolution: ~150 μm	Speed: up to 40 mm/s; Demonstrated in vivo near diseased mouse bladder areas and deep within rabbit leg muscles	In vivo/tissue examples: 7–24 W at 2.65 MHz, 10–20 mm/min	Frequency: 1.1, 2.65, 8.75 MHz; Single-element FUS (models H102, H108); Array geometry: single-element	Ultrasound ink = biopolymer + LTSL-encapsulated crosslinker; trigger: stable at 37 °C, releases at ~41.7 °C	Build volume limited by the injected volume and stage travel
Ultrasound-mediated polymerization[33]	Potential deep-body FUS resolution <1 mm	Full polymerization demonstrated through 1–3 cm thick tissues (muscle/brain)	37 kHz or 1 MHz; intensity 0.3–2.2 W/ cm^2; exposure 5–30 s; full polymerization in multiple conditions	Frequency: 37 kHz and 1 MHz (planar or focused); transducers: 1-MHz planar/ focused probes; 37-kHz sonicator	PEGDA or PVA-MA; can be enriched with ECM proteins/ minerals; exposure: 5/10/30 s; <1 min in some contexts	Build volume: tissue thickness 1–3 cm; max part size not quantified

Abbreviations: APS: Ammonium persulfate; DSP: Direct sound printing; ECM: Extracellular matrix; FWHM: Full width at half maximum; HDSP: Holographic direct sound printing; HEA: 2-hydroxyethyl acrylate; HIFU: High-intensity focused ultrasound; LTSL: Low-temperature–sensitive liposomes; PDMS: Polydimethylsiloxane; PEGDA: Polyethylene glycol diacrylate; PNIPAm: Poly(N-isopropylacrylamide); PU: Polyurethane.

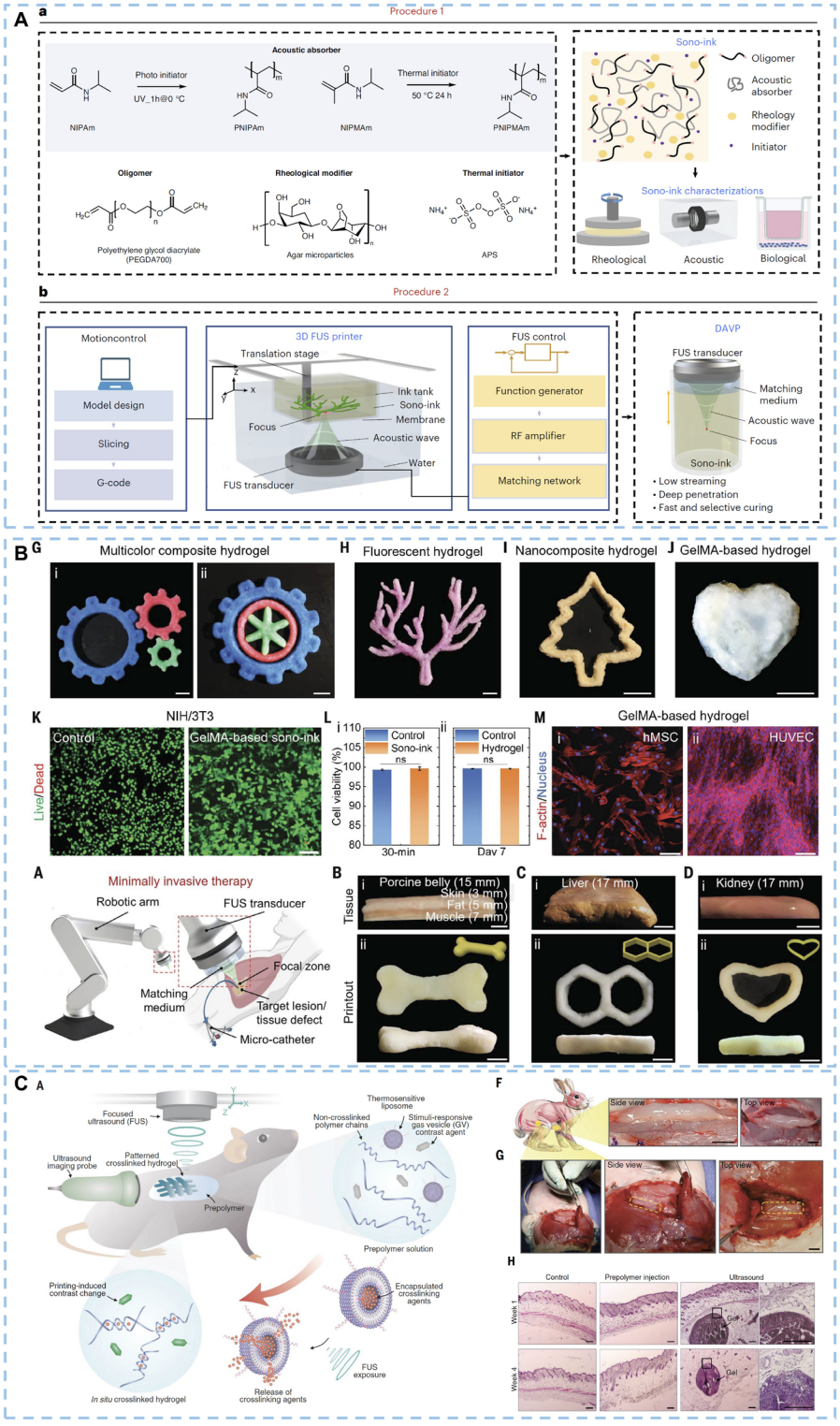

Figure 6. Acoustic-assisted 3D bioprinting. (A) Bioink composition, working principle, setup, and printing process of deep-penetration acoustic volumetric bioprinting (DAVP). Reprinted with permission from Kuang *et al.*[130] Copyright © 2025, Nature Portfolio. (B) Photographs of *ex vivo* printing constructs and the *in vivo* model printing process using DAVP. Reprinted with permission from Kuang *et al.*[128] Copyright © 2023, AAAS. (C) Schematic of the acoustic printing platform based on low-temperature–sensitive liposomes and the results of its deep-tissue penetration printing *in vivo*. Reprinted with permission from Davoodi *et al.*[133] Copyright © 2025, AAAS.

5. Conclusion

This review highlights the significant potential and innovative mechanisms of ultrasound as a unique physical stimulus in the fields of hydrogel fabrication, 3D printing, and 3D bioprinting. Compared to traditional external stimuli (e.g., light, heat), ultrasound—by virtue of its diverse physicochemical effects—offers distinct advantages, including deep tissue penetration, high spatiotemporal controllability, good biocompatibility, and often milder processing conditions, driving the field toward more profound, precise, and clinically relevant applications.

In summary, recent studies have successfully elucidated multiple pathways for ultrasound-triggered hydrogel formation, each offering distinct advantages in terms of gelation kinetics, biocompatibility, material applicability, and spatiotemporal controllability. Among these, cavitation effects and ultrasound-triggered self-assembly systems enable rapid gelation, typically completing within tens of seconds to a few minutes, rendering them suitable for applications requiring rapid in situ solidification. In contrast, enzymatic and liposome-mediated gelation strategies exhibit longer gelation times, ranging from several minutes to tens of minutes.

Nevertheless, ultrasound can function as a "remote switch" by stimulating responsive carriers (e.g., liposomes) to release enzymes, ions, or crosslinkers on demand, thereby enabling precise modulation of crosslinking dynamics and achieving highly biocompatible gelation through an indirect mechanism. This confers unique advantages on these strategies in cell encapsulation and tissue engineering. Mechanistically, mechanical and thermal effects primarily contribute to the rearrangement of polymer chains and the densification of network structures, while ultrasonic homogenization plays an auxiliary role in enhancing dispersion and optimizing structural uniformity. Notably, mechanisms such as acoustic streaming induced by SAWs and acoustic droplet vaporization enable spatiotemporal control over gel formation and subsequent properties, facilitating the construction of hydrogels with structural gradients or locally tailored mechanical characteristics.

In the aspect of acoustic-assisted hydrogel fabrication, future research may adopt tailored methodologies based on specific application scenarios. Although considerable progress has been made in elucidating the mechanisms underlying ultrasound-mediated hydrogel formation, current understanding remains largely qualitative. Future efforts should prioritize the application of advanced in situ characterization techniques to probe the interplay between cavitation effects and polymer crosslinking. In particular, the synergistic effects between mechanical and thermal perturbations remain insufficiently resolved. Moreover, accurately predicting optimal ultrasound parameters (e.g., frequency, intensity, duty cycle) based on material properties remains a critical challenge. The establishment of a comprehensive structure–property relationship database correlating ultrasound parameters with hydrogel performance would facilitate the transition from empirical knowledge to data-driven guidance, substantially enhancing research efficiency and accuracy.

At the forefront of 3D printing and 3D bioprinting, acoustic-assisted technologies are overcoming the inherent limitations of conventional methods. Predominant techniques such as extrusion-based and vat photopolymerization face challenges in printing resolution, cell-friendliness, and crucially, the capability for in situ biomanufacturing. The evolution from millimeter-scale printing via cavitation-based radical polymerization, to penetration-capable volumetric printing using FUS-induced thermal effects with self-enhancing phase-transition inks, and most recently to sub-millimeter resolution printing via a low-temperature trigger strategy based on LTSLs, marks a clear trajectory toward transforming the paradigm from "construct-then-implant" to "*in situ* precise construction." The ultimate goal is to deliver bioinks to deep target tissues percutaneously or minimally invasively, then utilize ultrasound's penetration and focusing capabilities to directly print biocompatible, functional tissue repair scaffolds conforming to the defect morphology *in vivo*.

Acoustic-assisted 3D printing and 3D bioprinting are transitioning from "proof-of-feasibility" to a stage where engineering performance boundaries and translational viability are the central focus. Representative studies, employing different mechanistic approaches, have demonstrated: (i) feature sizes in the hundreds of micrometers (e.g., reported line widths/minimum features in the 100–300 μm range); and (ii) centimeter-scale energy delivery through tissue/scattering media to enable in situ gelation/curing (e.g., maintaining printability under 15–40 mm tissue coverage, or achieving focal-zone temperature elevation to 60–80 °C within seconds at <100 W input power). However, these results also clearly expose a tightly coupled relationship among resolution–penetration depth–throughput–energy–biosafety, making them difficult to optimize simultaneously. For example, in deep-penetration situations, thermal diffusion and acoustic streaming can broaden the theoretical focal spot into millimeter-scale cured dimensions, with pronounced anisotropy. In cavitation-triggered polymerization, increasing power can markedly raise streaming velocity and degrade shape fidelity.

Currently, the primary bottleneck limiting acoustic-assisted hydrogel fabrication, 3D printing, and 3D bioprinting is biosafety concerns associated with these processes. Ultrasound action, particularly cavitation and thermal effects, may cause unintended damage to bioactive macromolecules, and the degradation products of hydrogels applied *in vivo* require more systematic safety evaluation. Moreover, when hydrogels are intended for cell encapsulation, cell viability may be compromised by ultrasound exposure. A significant challenge lies in optimizing acoustic parameters to ensure robust fabrication outcomes while preserving high cell viability. Additional hurdles include balancing fabrication resolution with structural complexity, pushing the boundaries of printability, expanding the library of ultrasound-responsive bioinks, and establishing standardized protocols for these emerging manufacturing processes.

Future efforts should focus on several key directions. First, acoustic-assisted 3D printing and 3D bioprinting currently lack unified reporting standards and key data, particularly regarding acoustic field design and energy parameters, making rigorous quantitative comparison and replication across different studies challenging. Inconsistencies in terminology and unclear quantitative boundaries also persist: resolution is often ambiguously referred to as either "acoustic focal spot" or "cured line width," and throughput metrics lack a standardized definition. These parameters urgently require systematic establishment and standardization. Second, further theoretical and experimental investigation into the fundamental interactions between acoustic fields and materials is needed to guide the rational design of both sound fields and hydrogel systems. Third, developing novel acoustic-responsive biomaterials, particularly hydrogel systems with additional desirable properties, is crucial. Fourth, research should be directed toward specific clinical applications that best leverage ultrasound's unique advantages, such as repairing deep-seated or surgically inaccessible tissue defects or irregular cavity-shaped organs, thereby driving the design of tailored material systems and complete therapeutic workflows. Finally, rigorous standardization of acoustic-assisted hydrogel fabrication and 3D bioprinting technologies is essential to facilitate their transition from promising laboratory innovations to transformative tools with significant impact in biomedicine.

Acknowledgments

None.

Funding

This study was funded by the National Natural Science Foundation of China (W2511096 and 82572246) and the Sichuan Science and Technology Program (2026NSFSC1782 and 2026NSFSC1784).

Conflict of interest

The authors declare no known financial conflicts of interest or personal relationships relevant to this article.

Author contributions

Conceptualization: Zichuan Ding, Li Qiu
Data curation: Zichuan Ding, Yiyuan Wang
Funding acquisition: Zichuan Ding, Xiao Rong, Li Qiu
Investigation: Zichuan Ding, Xiao Rong, Yiyuan Wang
Methodology: Zichuan Ding, Xiao Rong, Ying Hong
Visualization: Xiao Rong
Supervision: Xiao Rong, Li Qiu
Writing–original draft: Zichuan Ding, Yiyuan Wang
Writing–review & editing: Xiao Rong, Li Qiu

Ethics approval and consent to participate

Not applicable.

Consent for publication

Not applicable.

Availability of data

Not applicable.

References

1. Dong S, An S, Saiding Q, *et al*. Therapeutic Hydrogels: Properties and Biomedical Applications. *Chem Rev*. 2025;125(18):8835-8920.

   doi: 10.1021/acs.chemrev.5c00182

2. Chen L, Jin Z, Feng W, Sun L, Xu H, Wang C. A hyperelastic hydrogel with an ultralarge reversible biaxial strain. *Science*. 2024;383(6690):1455-1461.

   doi: 10.1126/science.adh3632

3. Gao Y, Peng K, Mitragotri S. Covalently Crosslinked Hydrogels via Step-Growth Reactions: Crosslinking Chemistries, Polymers, and Clinical Impact. *Adv Mater*. 2021;33(25).

   doi: 10.1002/adma.202006362

4. Goswami AK, Giduturi VK, Yerramilli SN, Chauhan VS, Yadav N. Tissue engineering: Hydrogel scaffolds and mechanical properties as key design parameters. *Adv Colloid*

Interface Sci. 2026;347:103691.

doi: 10.1016/j.cis.2025.103691

5. Chen G, Yang Z, Pan H, *et al*. A Review of Hydrogel Fiber: Design, Synthesis, Applications, and Futures. *Chem Rev*. 2025;125(13):5991-6056.

doi: 10.1021/acs.chemrev.5c00159

6. Yin Y, Gu Q, Liu X, Liu F, McClements DJ. Double network hydrogels: Design, fabrication, and application in biomedicines and foods. *Adv Colloid Interface Sci*. 2023;320:102999.

doi: 10.1016/j.cis.2023.102999

7. Ding Z, Liang Z, Rong X, *et al*. Janus-Structured Microgel Barrier with Tissue Adhesive and Hemostatic Characteristics for Efficient Prevention of Postoperative Adhesion. *Small*. 2024;20(50).

doi: 10.1002/smll.202403753

8. Fan J, Ding Z, Cai Y, *et al*. Revolutionizing Bone Regeneration: Vascularized Bone Tissue Engineering with Advanced 3D Printing Technology. *Aggregate*. 2025;6(4).

doi: 10.1002/agt2.731

9. Wu X, Shi W, Liu X, Gu Z. Recent advances in 3D-printing-based organ-on-a-chip. *EngMedicine*. 2024;1(1):100003.

doi: 10.1016/j.engmed.2024.100003

10. Hu L, Chee PL, Sugiarto S, *et al*. Hydrogel-Based Flexible Electronics. *Adv Mater*. 2023;35(14).

doi: 10.1002/adma.202205326

11. Wang M, Li W, Hao J, *et al*. Biomaterial-minimalistic photoactivated bioprinting of cell-dense tissues. *Cell*. 2026;189(1):106-122.e26.

doi: 10.1016/j.cell.2025.11.012

12. Rong X, Xiao S, Geng W, *et al*. Sono-activable and biocatalytic 3D-printed scaffolds for intelligently sequential therapies in osteosarcoma eradication and defect regeneration. *Nat Commun*. 2025;16(1).

doi: 10.1038/s41467-025-61377-x

13. Yi HG, Kim H, Kwon J, Choi YJ, Jang J, Cho DW. Application of 3D bioprinting in the prevention and the therapy for human diseases. *Signal Transduct Target Ther*. 2021;6(1).

doi: 10.1038/s41392-021-00566-8

14. Lee SJ, Jeong W, Atala A. 3D Bioprinting for Engineered Tissue Constructs and Patient-Specific Models: Current Progress and Prospects in Clinical Applications. *Adv Mater*. 2024;36(49).

doi: 10.1002/adma.202408032

15. Luo Z, Tang G, Ravanbakhsh H, *et al*. Vertical Extrusion Cryo(bio)printing for Anisotropic Tissue Manufacturing. *Adv Mater*. 2022;34(12).

doi: 10.1002/adma.202108931

16. Chen Z, Zhang H, Huang J, *et al*. DNA-encoded dynamic hydrogels for 3D bioprinted cartilage organoids. *Mater Today Bio*. 2025;31:101509.

doi: 10.1016/j.mtbio.2025.101509

17. Burns N, Rajesh A, Manjula-Basavanna A, Duraj-Thatte A. 3D extrusion bioprinting of microbial inks for biomedical applications. *Adv Drug Deliv Rev*. 2025;217:115505.

doi: 10.1016/j.addr.2024.115505

18. Li S, Li J, Xu J, *et al*. Removal-Free and Multicellular Suspension Bath-Based 3D Bioprinting. *Adv Mater*. 2024;36(48).

doi: 10.1002/adma.202406891

19. Jeong YG, Yoo JJ, Lee SJ, Kim MS. 3D digital light process bioprinting: Cutting-edge platforms for resolution of organ fabrication. *Mater Today Bio*. 2024;29:101284.

doi: 10.1016/j.mtbio.2024.101284

20. Wang M, Li W, Hao J, *et al*. Molecularly cleavable bioinks facilitate high-performance digital light processing-based bioprinting of functional volumetric soft tissues. *Nat Commun*. 2022;13(1).

doi: 10.1038/s41467-022-31002-2

21. Chen Y, Zhang J, Liu X, *et al*. Noninvasive in vivo 3D bioprinting. *Sci Adv*. 2020;6(23).

doi: 10.1126/sciadv.aba7406

22. Murphy SV, De Coppi P, Atala A. Opportunities and challenges of translational 3D bioprinting. *Nat Biomed Eng*. 2020;4(4):370-380.

doi: 10.1038/s41551-019-0471-7

23. Wu J, Gao Y, Zhou H, *et al*. Ultrasound-enhanced gene transfection: vectors, methods, and biomedical applications. *Ultrason Sonochem*. 2025;122:107607.

doi: 10.1016/j.ultsonch.2025.107607

24. Zhao H, Du F, Xiang X, *et al*. Progress in application of nanomedicines for enhancing cancer sono-immunotherapy. *Ultrason Sonochem*. 2024;111:107105.

doi: 10.1016/j.ultsonch.2024.107105

25. Jiang H, Ye L, Yuan X, Luo Q, Zhou N, Hu B. Endoscopic ultrasound-based artificial intelligence for gastrointestinal subepithelial lesions. *EngMedicine*. 2025;2(2):100073.

doi: 10.1016/j.engmed.2025.100073

26. Athanassiadis AG, Ma Z, Moreno-Gomez N, *et al*. Ultrasound-Responsive Systems as Components for Smart Materials. *Chem Rev*. 2022;122(5):5165-5208.

doi: 10.1021/acs.chemrev.1c00622

27. Chen S, Ouyang Q, Miao X, *et al*. Wearable Ultrasound Devices for Therapeutic Applications. *Nano-Micro Lett*.

2025;18(1).

doi: 10.1007/s40820-025-01890-2

28. Cass P, Knower W, Pereeia E, Holmes NP, Hughes T. Preparation of hydrogels via ultrasonic polymerization. *Ultrason Sonochem*. 2010;17(2):326-332.

doi: 10.1016/j.ultsonch.2009.08.008

29. Heng BC, Li X, Guo Y, *et al*. Biophysical stimuli for promoting angiogenesis and vascularization in regenerative medicine and dentistry. *EngMedicine*. 2025;2(3):100078.

doi: 10.1016/j.engmed.2025.100078

30. Poolman RW, Agoritsas T, Siemieniuk RA, *et al*. Low intensity pulsed ultrasound (LIPUS) for bone healing: a clinical practice guideline. *BMJ*. 2017;356:j576.

doi: 10.1136/bmj.j576

31. Zheng H, Zuo B. Functional silk fibroin hydrogels: preparation, properties and applications. *J Mater Chem B*. 2021;9(5):1238-1258.

doi: 10.1039/D0TB02099K

32. Santha Kumar ARS, Padmakumar A, Kalita U, *et al*. Ultrasonics in polymer science: applications and challenges. *Prog Mater Sci*. 2023;136:101113.

doi: 10.1016/j.pmatsci.2023.101113

33. Garciamendez-Mijares CE, Ruiz DSR, Kuang X, *et al*. Acoustic Bioprinting: A Glimpse Into an Emerging Field. *Small Methods*. 2025;10(3).

doi: 10.1002/smtd.202500733

34. Mondal J, Lakkaraju R, Ghosh P, Ashokkumar M. Acoustic cavitation-induced shear: a mini-review. *Biophys Rev*. 2021;13(6):1229-1243.

doi: 10.1007/s12551-021-00896-5

35. Zhu X, Das RS, Bhavya ML, Garcia-Vaquero M, Tiwari BK. Acoustic cavitation for agri-food applications: Mechanism of action, design of new systems, challenges and strategies for scale-up. *Ultrason Sonochem*. 2024;105:106850.

doi: 10.1016/j.ultsonch.2024.106850

36. Yusof NS, Babgi B, Alghamdi Y, Aksu M, Madhavan J, Ashokkumar M. Physical and chemical effects of acoustic cavitation in selected ultrasonic cleaning applications. *Ultrason Sonochem*. 2016;29:568-576.

doi: 10.1016/j.ultsonch.2015.06.013

37. Abbott JG. Rationale and derivation of MI and TI--a review. *Ultrasound Med Biol*. 1999;25(3):431-441.

doi: 10.1016/s0301-5629(98)00172-0

38. Lenshof A, Magnusson C, Laurell T. Acoustofluidics 8: Applications of acoustophoresis in continuous flow microsystems. *Lab Chip*. 2012;12(7):1210-1223.

doi: 10.1039/c2lc21256k

39. Padilla F, Brenner J, Prada F, Klibanov AL. Theranostics in the vasculature: bioeffects of ultrasound and microbubbles to induce vascular shutdown. *Theranostics*. 2023;13(12):4079-4101.

doi: 10.7150/thno.70372

40. Coussios CC, Roy RA. Applications of Acoustics and Cavitation to Noninvasive Therapy and Drug Delivery. *Annu Rev Fluid Mech*. 2008;40(1):395-420.

doi: 10.1146/annurev.fluid.40.111406.102116

41. Church CC, Carstensen EL. "Stable" inertial cavitation. *Ultrasound Med Biol*. 2001;27(10):1435-1437.

doi: 10.1016/s0301-5629(01)00441-0

42. Lighthill SJ. Acoustic streaming. *J Sound Vib*. 1978;61(3):391-418.

doi: 10.1016/0022-460X(78)90388-7

43. Eckart C. Vortices and Streams Caused by Sound Waves. *Phys Rev*. 1948;73(1):68-76.

doi: 10.1103/PhysRev.73.68

44. Wiklund M, Green R, Ohlin M. Acoustofluidics 14: Applications of acoustic streaming in microfluidic devices. *Lab Chip*. 2012;12(14):2438-2451.

doi: 10.1039/C2LC40203C

45. Sirsi SR, Borden MA. State-of-the-art materials for ultrasound-triggered drug delivery. *Adv Drug Deliv Rev*. 2014;72:3-14.

doi: 10.1016/j.addr.2013.12.010

46. Liu Y, Yin Q, Luo Y, *et al*. Manipulation with sound and vibration: A review on the micromanipulation system based on sub-MHz acoustic waves. *Ultrason Sonochem*. 2023;96:106441.

doi: 10.1016/j.ultsonch.2023.106441

47. Li Y, Qiu C, Xu S, Ke M, Liu Z. Theoretical Study of Large-Angle Bending Transport of Microparticles by 2D Acoustic Half-Bessel Beams. *Sci Rep*. 2015;5(1).

doi: 10.1038/srep13063

48. Duan L, Yang L, Jin J, *et al*. Micro/nano-bubble-assisted ultrasound to enhance the EPR effect and potential theranostic applications. *Theranostics*. 2020;10(2):462-483.

doi: 10.7150/thno.37593

49. Gor'kov LP. On the forces acting on a small particle in an acoustical field in an ideal fluid. In: *Selected Papers of Lev P Gor'kov*. World Scientific Publishing Co.; 2014:307-317.

doi: 10.1142/9789814366960_0008

50. Kolesnik K, Xu M, Lee PVS, Rajagopal V, Collins DJ. Unconventional acoustic approaches for localized and designed micromanipulation. *Lab Chip*. 2021;21(15):2837-2856.

doi: 10.1039/D1LC00378J

51. Zhu L, Altman MB, Laszlo A, *et al*. Ultrasound Hyperthermia Technology for Radiosensitization. *Ultrasound Med Biol*. 2019;45(5):1025-1043.

doi: 10.1016/j.ultrasmedbio.2018.12.007

52. O'Reilly MA. Exploiting the mechanical effects of ultrasound for noninvasive therapy. *Science*. 2024;385(6714).

doi: 10.1126/science.adp7206

53. Kok HP, Cressman ENK, Ceelen W, *et al*. Heating technology for malignant tumors: a review. *Int J Hyperthermia*. 2020;37(1):711-741.

doi: 10.1080/02656736.2020.1779357

54. Arthur RM, Straube WL, Trobaugh JW, Moros EG. Non-invasive estimation of hyperthermia temperatures with ultrasound. *Int J Hyperthermia*. 2005;21(6):589-600.

doi: 10.1080/02656730500159103

55. Ebrahimi R. Radiation initiated synthesis, characterization, and swelling behavior of poly (acrylic acid-co-acrylamide)/ starch grafted hydrogel. *J Appl Polym Sci*. 2021;138(37).

doi: 10.1002/app.50931

56. Xu PY, Kumar Kankala R, Wang SB, Chen AZ. Sonodynamic therapy-based nanoplatforms for combating bacterial infections. *Ultrason Sonochem*. 2023;100:106617.

doi: 10.1016/j.ultsonch.2023.106617

57. Liu YH, Li SB, Wang ZY, Wang L. Ultrasound in cellulose-based hydrogel for biomedical use: From extraction to preparation. *Colloids Surf B Biointerfaces*. 2022;212:112368.

doi: 10.1016/j.colsurfb.2022.112368

58. Velusamy M, Radhakrishnan M. Hydrogel fabrication using emerging technologies: Sources, mechanisms, and food applications. *Innov Food Sci Emerg Technol*. 2025;105:104226.

doi: 10.1016/j.ifset.2025.104226

59. Ebrahimi R, Niyaraki FS, Jirandeh AB. Ultrasonic Irradiated Synthesis of Acrylic Acid-co-Acrylamide as pH and Salt Sensitive Hydrogel. *J Polym Mater*. 2014;31(2):159-167. Available from: https://civilica.com/doc/244321/ [Last accessed on March 10, 2025].

60. Ebrahimi R, Ebrahimi M. The stimuli-response characters of hydrogels prepared using ultrasound. *J Polym Eng*. 2014;34(7):625-632.

doi: 10.1515/polyeng-2014-0028

61. Yang SR, Wang RB, Yan CJ, *et al*. Ultrasonic interfacial crosslinking of TiO2-based nanocomposite hydrogels through thiol-norbornene reactions for sonodynamic antibacterial treatment. *Biomater Sci*. 2023;11(12):4184-4199.

doi: 10.1039/d2bm01950g

62. Zhang L, Yao L, Zhao F, *et al*. Protein and Peptide-Based Nanotechnology for Enhancing Stability, Bioactivity, and Delivery of Anthocyanins. *Adv Healthc Mater*. 2023;12(25).

doi: 10.1002/adhm.202300473

63. Hilal A, Florowska A, Florowski T, *et al*. Effects of Sequential Induction Combining Thermal Treatment with Ultrasound or High Hydrostatic Pressure on the Physicochemical and Mechanical Properties of Pea Protein-Psyllium Hydrogels as Elderberry Extract Carriers. *Int J Mol Sci*. 2024;25(16):9033.

doi: 10.3390/ijms25169033

64. Ni Y, Wu JJ, Jiang YT, Li JW, Fan LP, Huang SQ. High-internal-phase pickering emulsions stabilized by ultrasound-induced nanocellulose hydrogels. *Food Hydrocolloids*. 2022;125:107395.

doi: 10.1016/j.foodhyd.2021.107395

65. Liu ZJ, Khurshid K, Saldaña MDA. Hydrogels and aerogels of cellulose nanofiber derived from barley straw with addition of chitosan using high-intensity ultrasound and supercritical CO2 drying. *Ind Crops Prod*. 2024;216:118755.

doi: 10.1016/j.indcrop.2024.118755

66. Rokita B, Rosiak JM, Ulanski P. Ultrasound-Induced Cross-Linking and Formation of Macroscopic Covalent Hydrogels in Aqueous Polymer and Monomer Solutions. *Macromolecules*. 2009;42(9):3269-3274.

doi: 10.1021/ma802565p

67. Rahmani N, Ebrahimi R. Removal Kinetics of Methylene Blue from Aquatic Medium using Hydrogel Nanocomposite Prepared by Ultrasound. *Water Air Soil Pollut*. 2024;235(9).

doi: 10.1007/s11270-024-07383-z

68. Ching TW, Haritos V, Tanksale A. Ultrasound-assisted conversion of cellulose into hydrogel and functional carbon material. *Cellulose*. 2018;25(4):2629-2645.

doi: 10.1007/s10570-018-1746-y

69. Cheng YX, Lee S, Xiao YH, *et al*. Ultrasound Cavitation Enables Rapid, Initiator-Free Fabrication of Tough Anti-Freezing Hydrogels. *Adv Sci*. 2025;12(22).

doi: 10.1002/advs.202416844

70. Jonnalagadda US, Nguyen TM, Li FF, *et al*. Sol-Gel Transitions of Comb-Like Polymethacrylate Copolymers by Mechano-Thermal Stimuli in Water. *Macromol Chem Phys*. 2020;221(13).

doi: 10.1002/macp.202000088

71. Norris EG, Dalecki D, Hocking DC. Acoustic Fabrication of Collagen-Fibronectin Composite Gels Accelerates Microtissue Formation. *Appl Sci*. 2020;10(8):2907.

doi: 10.3390/app10082907

72. Norris EG, Dalecki D, Hocking DC. Acoustic modification of collagen hydrogels facilitates cellular remodeling. *Mater*

Today Bio. 2019;3:100018.

doi: 10.1016/j.mtbio.2019.100018

73. Karamikamkar S, Behzadfar E, Cheung KC. A novel approach to producing uniform 3-D tumor spheroid constructs using ultrasound treatment. *Biomed Microdevices*. 2018;20(2).

doi: 10.1007/s10544-018-0260-1

74. Su H, Zheng ZC, Li LM, *et al*. Strategy for regulating hydrogel pore size through ultrasound-assisted directional freezing for enhanced interfacial evaporation. *Chem Eng J*. 2025;518:164731.

doi: 10.1016/j.cej.2025.164731

75. Nele V, Schutt CE, Wojciechowski JP, *et al*. Ultrasound-Triggered Enzymatic Gelation. *Adv Mater*. 2020;32(7).

doi: 10.1002/adma.201905914

76. Zhao ZY, Zhang Y, Meng C, Xie XY, Cui WG, Zuo KQ. Tissue-Penetrating Ultrasound-Triggered Hydrogel for Promoting Microvascular Network Reconstruction. *Adv Sci*. 2024;11(23).

doi: 10.1002/advs.202401368

77. Nele V, Wojciechowski JP, Armstrong JPK, Stevens MM. Tailoring Gelation Mechanisms for Advanced Hydrogel Applications. *Adv Funct Mater*. 2020;30(42).

doi: 10.1002/adfm.202002759

78. Xiong WF, Wang YT, Zhang CL, *et al*. High intensity ultrasound modified ovalbumin: Structure, interface and gelation properties. *Ultrason Sonochem*. 2016;31:302-309.

doi: 10.1016/j.ultsonch.2016.01.014

79. Wang YH, Liu Q, Yang YY, Zhang RX, Jiao AQ, Jin ZY. Construction of transglutaminase covalently cross-linked hydrogel and high internal phase emulsion gel from pea protein modified by high-intensity ultrasound. *J Sci Food Agric*. 2022;103(4):1874-1884.

doi: 10.1002/jsfa.12372

80. Bashash M, Varidi M, Varshosaz J. Ultrasound-triggered transglutaminase-catalyzed egg white-bovine gelatin composite hydrogel: Physicochemical and rheological studies. *Innov Food Sci Emerg Technol*. 2022;76:102936.

doi: 10.1016/j.ifset.2022.102936

81. Huerta RR, Silva EK, Ekaette I, El-Bialy T, Saldaña MDA. High-intensity ultrasound-assisted formation of cellulose nanofiber scaffold with low and high lignin content and their cytocompatibility with gingival fibroblast cells. *Ultrason Sonochem*. 2020;64:104759.

doi: 10.1016/j.ultsonch.2019.104759

82. Shulman LP. Miscarriage risk from amniocentesis performed for abnormal maternal serum screening. *Yearb Obstet Gynecol Womens Health*. 2008;2008:36-38.

doi: 10.1016/s1090-798x(08)79190-2

83. Chen B, Fragal EH, Faudry E, Halila S. In Situ Growth of Silver Nanoparticles into Reducing-End Carbohydrate-Based Supramolecular Hydrogels for Antimicrobial Applications. *ACS Appl Mater Interfaces*. 2024;16(51):70818-70827.

doi: 10.1021/acsami.4c17526

84. Streich C, Stein F, Jakobi J, *et al*. The Origin of the Intracellular Silver in Bacteria: A Comprehensive Study using Targeting Gold-Silver Alloy Nanoparticles. *Adv Healthc Mater*. 2023;12(30).

doi: 10.1002/adhm.202302084

85. Ling LY, Zhu L, Li YB, Liu CH, Cheng LX. Ultrasound-Induced Amino Acid-Based Hydrogels With Superior Mechanical Strength for Controllable Long-Term Release of Anti-Cercariae Drug. *Front Bioeng Biotechnol*. 2021;9.

doi: 10.3389/fbioe.2021.703582

86. Pan SF, Luo S, Li S, *et al*. Ultrasound accelerated gelation of novel L-lysine based hydrogelators. *Chem Commun*. 2013;49(73):8045.

doi: 10.1039/c3cc44767g

87. Xie ZG, Zhang AY, Ye L, Feng ZG. Organo- and hydrogels derived from cyclo(L-Tyr-L-Lys) and its ε-amino derivatives. *Soft Matter*. 2009;5(7):1474.

doi: 10.1039/b816664a

88. Ma ZC, Zhang P, Yu XD, *et al*. Sugar based nanotube assembly for the construction of sonication triggered hydrogel: an application of the entrapment of tetracycline hydrochloride. *J Mater Chem B*. 2015;3(37):7366-7371.

doi: 10.1039/c5tb01191d

89. Roy B, Bairi P, Nandi AK. Metastability in a bi-component hydrogel of thymine and 6-methyl-1,3,5-triazine-2,4-diamine: ultrasound induced vs. thermo gelation. *Soft Matter*. 2012;8(8):2366.

doi: 10.1039/c2sm07225d

90. Mallakpour S, Tabesh F. Tragacanth gum based hydrogel nanocomposites for the adsorption of methylene blue: Comparison of linear and non-linear forms of different adsorption isotherm and kinetics models. *Int J Biol Macromol*. 2019;133:754-766.

doi: 10.1016/j.ijbiomac.2019.04.129

91. Qu XY, Zhao Y, Chen ZA, *et al*. Thermoresponsive Lignin-Reinforced Poly(Ionic Liquid) Hydrogel Wireless Strain Sensor. *Research*. 2021;2021.

doi: 10.34133/2021/9845482

92. Khan SA, Siddiqui MF, Khan TA. Ultrasonic-assisted synthesis of polyacrylamide/bentonite hydrogel nanocomposite for the sequestration of lead and cadmium from aqueous phase: Equilibrium, kinetics and thermodynamic studies. *Ultrason Sonochem*. 2020;60:104761.

doi: 10.1016/j.ultsonch.2019.104761

93. Sun WX, Bu KX, Meng HM, Zhu CH. Hawthorn pectin/soybean isolate protein hydrogel bead as a promising ferrous ion-embedded delivery system. *Colloids Surf B Biointerfaces*. 2024;237:113867.

doi: 10.1016/j.colsurfb.2024.113867

94. Taktak F, Gökçe S. Ultrasound-assisted synthesis of biodegradable graphene oxide-based hydrogel nanocomposites for highly efficient and cost-effective removal of methyl orange from aqueous media. *J Water Process Eng*. 2024;58:104837.

doi: 10.1016/j.jwpe.2024.104837

95. Mohammadinezhad A, Marandi GB, Farsadrooh M, Javadian H. Synthesis of poly(acrylamide-co-itaconic acid)/MWCNTs superabsorbent hydrogel nanocomposite by ultrasound-assisted technique: Swelling behavior and Pb (II) adsorption capacity. *Ultrason Sonochem*. 2018;49:1-12.

doi: 10.1016/j.ultsonch.2017.12.028

96. Kang B, Shin J, Kang D, *et al*. Spatial regulation of hydrogel polymerization reaction using ultrasound-driven streaming vortex. *Ultrason Sonochem*. 2024;110:107053.

doi: 10.1016/j.ultsonch.2024.107053

97. Guo JB, Li YJ, Zhang YJ, Ren JJ, Yu XD, Cao XH. Switchable Supramolecular Configurations of Al3+/LysTPY Coordination Polymers in a Hydrogel Network Controlled by Ultrasound and Heat. *ACS Appl Mater Interfaces*. 2021;13(33):40079-40087.

doi: 10.1021/acsami.1c10150

98. Farrell E, Aliabouzar M, Quesada C, *et al*. Spatiotemporal control of myofibroblast activation in acoustically-responsive scaffolds via ultrasound-induced matrix stiffening. *Acta Biomater*. 2022;138:133-143.

doi: 10.1016/j.actbio.2021.11.020

99. Ebrahimi R. The study of factors affecting the swelling of ultrasound-prepared hydrogel. *Polym Bull*. 2019;76(2):1023-1039.

doi: 10.1007/s00289-018-2423-x

100. Hooshvar M, Marandi GB, Nakhjiri MT. Collagen-Based Hydrogel Nanocomposite as Adsorbent for Methylene Blue and Crystal Violet Removal from Aqueous Solution: Isotherm, Kinetic, and Thermodynamic Studies. *Water Air Soil Pollut*. 2024;235(2).

doi: 10.1007/s11270-024-06971-3

101. Wang XH, Zhou ZL, Guo XW, He Q, Hao C, Ge CW. Ultrasonic-assisted synthesis of sodium lignosulfonate-grafted poly(acrylic acid-co-poly(vinyl pyrrolidone)) hydrogel for drug delivery. *RSC Adv*. 2016;6(42):35550-35558.

doi: 10.1039/c6ra03398a

102. Buxaderas E, Moglie Y, Figueroa AB, *et al*. Ultrasound-Enhanced Gelation of Stimuli-Responsive and Biocompatible Phenylalanine-Derived Hydrogels. *Gels*. 2025;11(3):160.

doi: 10.3390/gels11030160

103. Zhu JW, Wang XR, Yang DL, *et al*. Ultrasound-Triggered In Situ Gelation to Overcome Tumor Hypoxia for Enhanced Photodynamic and Sustained Chemotherapy. *Adv Ther*. 2021;4(7).

doi: 10.1002/adtp.202100052

104. Li KY, Liu Y, Ge YQ, *et al*. An ultrasound-induced MXene doped PAM-SA super-tough hydrogel. *J Mater Chem C*. 2023;11(5):1908-1918.

doi: 10.1039/d2tc04665b

105. Zhang YS, Jiang RL, Fang A, *et al*. A highly transparent, elastic, injectable sericin hydrogel induced by ultrasound. *Polym Test*. 2019;77:105890.

doi: 10.1016/j.polymertesting.2019.05.006

106. Bardajee GR, Azimi S, Sharifi M. Ultrasonically accelerated synthesis of silver nanocomposite hydrogel based on salep biopolymer: application in Rhodamine dye adsorption. *Iran Polym J*. 2016;25(12):1047-1063.

doi: 10.1007/s13726-016-0490-0

107. Jiang CL, Wang XH, Wang GH, Hao C, Li X, Li TH. Adsorption performance of a polysaccharide composite hydrogel based on crosslinked glucan/chitosan for heavy metal ions. *Compos Part B Eng*. 2019;169:45-54.

doi: 10.1016/j.compositesb.2019.03.082

108. Mekala S, Silva EK, Saldaña MDA. Ultrasound-assisted production of emulsion-filled pectin hydrogels to encapsulate vitamin complex: Impact of the addition of xylooligosaccharides, ascorbic acid and supercritical CO2 drying. *Innov Food Sci Emerg Technol*. 2022;76:102907.

doi: 10.1016/j.ifset.2021.102907

109. Nakhjiri MT, Marandi GB, Kurdtabar M. Preparation of magnetic double network nanocomposite hydrogel for adsorption of phenol and p-nitrophenol from aqueous solution. *J Environ Chem Eng*. 2021;9(2):105039.

doi: 10.1016/j.jece.2021.105039

110. Bethi B, Manasa V, Srinija K, Sonawane SH. Intensification of Rhodamine-B dye removal using hydrodynamic cavitation coupled with hydrogel adsorption. *Chem Eng Process Process Intensif*. 2018;134:51-57.

doi: 10.1016/j.cep.2018.10.017

111. Shirsath SR, Hage AP, Zhou M, Sonawane SH, Ashokkumar M. Ultrasound assisted preparation of nanoclay Bentonite-FeCo nanocomposite hybrid hydrogel: A potential responsive sorbent for removal of organic pollutant from water. *Desalination*. 2011;281:429-437.

doi: 10.1016/j.desal.2011.08.031

112. Shirsath SR, Patil AP, Patil R, Naik JB, Gogate PR, Sonawane SH. Removal of Brilliant Green from wastewater using conventional and ultrasonically prepared poly(acrylic acid) hydrogel loaded with kaolin clay: A comparative study. *Ultrason Sonochem*. 2013;20(3):914-923.

doi: 10.1016/j.ultsonch.2012.11.010

113. Wang XH, Hou HQ, Li YJ, Wang YY, Hao C, Ge CW. A novel semi-IPN hydrogel: Preparation, swelling properties and adsorption studies of Co (II). *J Ind Eng Chem*. 2016;41:82-90.

doi: 10.1016/j.jiec.2016.07.012

114. Wang XH, Wang YY, He SF, Hou HQ, Hao C. Ultrasonic-assisted synthesis of superabsorbent hydrogels based on sodium lignosulfonate and their adsorption properties for Ni2+. *Ultrason Sonochem*. 2018;40:221-229.

doi: 10.1016/j.ultsonch.2017.07.011

115. Matai I, Kaur G, Seyedsalehi A, McClinton A, Laurencin CT. Progress in 3D bioprinting technology for tissue/organ regenerative engineering. *Biomaterials*. 2020;226:119536.

doi: 10.1016/j.biomaterials.2019.119536

116. Ding Z, Cai Y, Sun H, *et al*. Janus hydrogel microrobots with bioactive ions for the regeneration of tendon-bone interface. *Nat Commun*. 2025;16(1).

doi: 10.1038/s41467-025-57499-x

117. Urciuolo A, Poli I, Brandolino L, *et al*. Intravital three-dimensional bioprinting. *Nat Biomed Eng*. 2020;4(9):901-915.

doi: 10.1038/s41551-020-0568-z

118. Xie M, Lian L, Mu X, *et al*. Volumetric additive manufacturing of pristine silk-based (bio)inks. *Nat Commun*. 2023;14(1).

doi: 10.1038/s41467-023-35807-7

119. Debbi L, Machour M, Dahis D, *et al*. Ultrasound Mediated Polymerization for Cell Delivery, Drug Delivery, and 3D Printing. *Small Methods*. 2024;8(7).

doi: 10.1002/smtd.202301197

120. An X, Yu W, Liu J, Tang D, Yang L, Chen X. Oxidative cell death in cancer: mechanisms and therapeutic opportunities. *Cell Death Dis*. 2024;15(8).

doi: 10.1038/s41419-024-06939-5

121. Suslick KS, Eddingsaas NC, Flannigan DJ, Hopkins SD, Xu H. The Chemical History of a Bubble. *Acc Chem Res*. 2018;51(9):2169-2178.

doi: 10.1021/acs.accounts.8b00088

122. Pokhrel N, Vabbina PK, Pala N. Sonochemistry: Science and Engineering. *Ultrason Sonochem*. 2016;29:104-128.

doi: 10.1016/j.ultsonch.2015.07.023

123. Yusof NSM, Anandan S, Sivashanmugam P, Flores EMM, Ashokkumar M. A correlation between cavitation bubble temperature, sonoluminescence and interfacial chemistry - A minireview. *Ultrason Sonochem*. 2022;85:105988.

doi: 10.1016/j.ultsonch.2022.105988

124. Habibi M, Foroughi S, Karamzadeh V, Packirisamy M. Direct sound printing. *Nat Commun*. 2022;13(1).

doi: 10.1038/s41467-022-29395-1

125. Derayatifar M, Habibi M, Bhat R, Packirisamy M. Holographic direct sound printing. *Nat Commun*. 2024;15(1).

doi: 10.1038/s41467-024-50923-8

126. Yao G, Xiang H, Lucas M, *et al*. Sound Continuous Production of Thermosets. *Adv Funct Mater*. 2024;34(12).

doi: 10.1002/adfm.202312736

127. Lee CU, Cui J, Tewani HR, Prabhakar P, Boydston AJ. Creation of three-dimensional composite architectures via high-intensity focused ultrasound inside of foams. *RSC Appl Polym*. 2024;2(4):692-700.

doi: 10.1039/d4lp00002a

128. Kuang X, Rong Q, Belal S, *et al*. Self-enhancing sono-inks enable deep-penetration acoustic volumetric printing. *Science*. 2023;382(6675):1148-1155.

doi: 10.1126/science.adi1563

129. Papadakis CM, Niebuur BJ, Schulte A. Thermoresponsive Polymers under Pressure with a Focus on Poly(N-isopropylacrylamide) (PNIPAM). *Langmuir*. 2023;40(1):1-20.

doi: 10.1021/acs.langmuir.3c02398

130. Kuang X, Rong Q, Belal S, *et al*. Sonicated inks and focused-ultrasound writing enable deep-penetration acoustic volumetric printing. *Nat Protoc*. Preprint posted online 2025.

doi: 10.1038/s41596-025-01258-1

131. Hakim Khalili M, Zhang R, Wilson S, Goel S, Impey SA, Aria AI. Additive Manufacturing and Physicomechanical Characteristics of PEGDA Hydrogels: Recent Advances and Perspective for Tissue Engineering. *Polymers*. 2023;15(10):2341.

doi: 10.3390/polym15102341

132. Zhou B, Jiang X, Zhou X, *et al*. GelMA-based bioactive hydrogel scaffolds with multiple bone defect repair functions: therapeutic strategies and recent advances. *Biomater Res*. 2023;27(1).

doi: 10.1186/s40824-023-00422-6

133. Davoodi E, Li J, Ma X, *et al*. Imaging-guided deep tissue in vivo sound printing. *Science*. 2025;388(6747):616-623.

doi: 10.1126/science.adt0293

134. Ta T, Porter TM. Thermosensitive liposomes for localized delivery and triggered release of chemotherapy. *J Control Release*. 2013;169(1-2):112-125.

doi: 10.1016/j.jconrel.2013.03.036

135. Needham D, Park J-Y, Wright AM, Tong J. Materials characterization of the low temperature sensitive liposome (LTSL): effects of the lipid composition (lysolipid and DSPE–PEG2000) on the thermal transition and release of doxorubicin. *Faraday Discuss*. 2013;161:515-534.

doi: 10.1039/C2FD20111A

136. Madhusudhan A, Suhagia TA, Sharma C, Jaganathan SK, Purohit SD. Carbon Based Polymeric Nanocomposite Hydrogel Bioink: A Review. *Polymers*. 2024;16(23):3318.

doi: 10.3390/polym16233318

137. Liu B, Chen J, Li Y, Ruan H, Cui W. Imaging-guided non-invasive in vivo acoustic printing: a new "surgery-as-printing" paradigm for precision medicine. *Sci China Life Sci*. 2025;69(4):1434-1437.

doi: 10.1007/s11427-025-3027-0